NASA Contractor Report 166041

THE MEASUREMENT OF THE SYNOPTIC SCALE WIND OVER THE OCEAN

Willard J. Pierson

CUNY INSTITUTE OF MARINE AND ATMOSPHERIC
SCIENCES AT THE CITY COLLEGE
New York, New York 10031

Contract NAS1-15669 and
Grant NAGW-266
December 1982

National Aeronautics and
Space Administration

Langley Research Center
Hampton, Virginia 23665

TABLE OF CONTENTS

INTRODUCTION

There are many different scales of motion in meteorology. They range from the trade winds that exist over the equatorial oceans between about 30^{o} N and 30^{o} S and extend all around the Earth, to the annually varying monsoon winds over Asia and the sub-continent of India, on through the semi-permanent subtropical high pressure cells and synoptic scale tropical and extratropical cyclones, to diurnal sea breeze circulations and mountain valley winds, on to tornadoes, dust devils and water spouts to cloud motions and the air motions therein and finally to various scales of turbulent motions ending with the Reynolds flux motions, the Kolmogorov inertial range and molecular viscosity. Fujita (1981) has cited fourteen different ways to categorize these various scales and proposed a fifteenth.

One commonly accepted scale is the mesoscale, but the mesoscale covers a wide range of frequencies and wavenumbers as illustrated by the recent special issue on mesoscale meteorology of the Journal of Atmospheric Sciences (August, Vol. 38 No, 8) and by many other papers such as the work of Clancy et al. (1979).

The horizontal and vertical scales of motion and the periods (or frequencies) involved that various authors ascribe to the mesoscale cover a wide range and are related to some clearly definable atmospheric event. There are many different kinds of mesoscale motions of great interest in themselves that are studied so that they can be better understood and even, perhaps, forecast in a general, or statistical, sense. Examples would be forecasts of tornadoes or severe thunderstorms for a particular area within a particular time interval.

Especially over the oceans, there is a scale of motion on the low frequency end of the microscale that extends to the synoptic scale and that cannot be resolved either by the conventional data buoy and ship of opportunity network or by potential remote sensing systems such as improved versions of the SEASAT scatterometer. The periods involved are wind speed dependent but range from more than one hour to several minutes. For want of a better term, this scale will be referred to as the mesoscale. It separates the conventionally defined synoptic scale from the microscale. There are no clearly definable atmospheric events of interest to meteorologists associated with these particular random fluctuations.

The mesoscale motions to be emphazised here are dominantly a nuisance factor and a bothersome aspect for both the correct analysis of the synoptic scale (because they disguise it) and for the interpretation of microscale measurements of the fluxes of momentum, heat and water vapor needed to close the equations of motion for the synoptic scale by means of the bulk aerodynamic equations. They are a poorly understood area of study because they are inadequately treated at both the synoptic scale and at the microscale. They introduce a source of variability, essentially errors in a statistical sense, in synoptic scale analyses. This error source can be removed by improved wind measurement methods that filter them out of the synoptic scale so that synoptic scale motions can be specified correctly for numerical weather prediction purposes.

The SEASAT scatterometer (SASS) measured winds by a remote sensing method. Some day a similar instrument may be used to measure the winds over the ocean globally on an operational basis. The comparison of the winds determined from the SASS with conventionally measured winds is made more difficult because of the presence of mesoscale eddies in both space and time that makes area averages of the winds from the SASS differ from time averages of anemometer winds for reasons other than instrumental measurement errors in either system.

Typically, present procedures average out (or filter out) all of the microscale and a small part of the mesoscale, but leave an additional part of the mesoscale in the resulting vector wind as a perturbation of a more representative synoptic scale value. The mesoscale and the microscale can be modeled as a function of the synoptic scale winds so as to determine the effect of different time and space averages on the determination of the vector wind. From this, some conclusions can be obtained concerning possible averaging times for anemometers and possible area averages for spacecraft systems.

The purposes of this paper are (1) to study the effects of mesoscale and microscale fluctuations of the winds on the determination of the synoptic scale wind, (2) to show the effects of mesoscale variability on the verification of wind forecasts and on the comparison of remotely sensed and anemometer averaged winds, and (3) to show how to measure the synoptic scale wind more accurately. Major conclusions are (1) that conventionally measured winds ought to be averaged for considerably longer times than at present, (2) that this averaging time is a function of synoptic scale conditions,(3) that spaceborne remote sensing devices can best be used to measure the synoptic scale,(4) that measurements of the wind made at nearly the some location and at nearly the same time can both be nearly correct and yet differ substantially because of unresolved mesoscale effects and (5) that attempts to get too high a spatial resolution by remote sensing may prove to be counter productive.

THE SYNOPTIC SCALE OVER THE OCEAN

A major objective of the science of meteorology is to forecast synoptic scale conditions over the Earth for as far as possible into the future and in particular for the 24, 48, 72 and 96 hour time frame. The equations that define the synoptic scale motions use time, and space, averaged values of the winds, or their equivalent, and of the other physical quantities in the equations. The effects of smaller scales of motion, often referred to as sub grid scales, are parameterized by various ingenious schemes. Much of the data that go into the initial value specifications are not the properly averaged value for the synoptic scale model being used. Models of the planetary boundary layer based on the Monin Obukov theory can be used to define the fluxes of momentum, heat and water vapor near the surface so that the synoptic scale equations of motion are completely defined in terms of the time and space averaged quantities.

The philosophy behind synoptic scale forecasts by numerical methods has been questioned by Robinson (1978a) and discussed by Laurmann (1978) with a reply by Robinson (1978b). The procedures in use do however actually give greatly improved forecasts compared to those of twenty or thirty years ago under some conditions. One of many examples is the report by Brown and Olson (1978). There are also examples of failures of the present methods as for example in the reports by Gyakum (1980) and Cane and Cardone (1981). Future improvements in synoptic scale forecasts will depend on higher speed computers, on improved physical models and on the more accurate specification of the initial value conditions for a forecast.

Procedures for the synoptic scale analysis of the field of mass and the field of motion over the oceans use both the sea surface pressure and the wind speed and direction reported by ships and buoys. These reports are few and far between and do not produce very accurate analyses for gradients, central pressures and the location of low centers. The reported winds are traditionally, and justifiably, treated as having large errors as described for the analysis procedures used by the National Meteorological Service in papers by McPherson, et al. (1979) and Bergman (1979). Analysis errors are believed to be a part of the reason for poor forecasts after about two days. If the winds could be measured for the synoptic scale more accurately, the analysis techniques could be extended to more realistic planetary boundary layer models and the winds could be assigned narrower error bounds so that the analysis could be improved.

A computer based numerical weather prediction requires an initial value specification of the field of mass and the field of motion of the atmosphere. This initial value specification is obtained by correcting a "first guess" field, based on a recent forecast computation, by means of the current "synoptic" observations. Almost by definition, and with perhaps a somewhat circular argument, the wind that ought to be measured by a ship, or a data buoy, or a spacecraft over the ocean ought to be that wind that will best

define the synoptic scale being forecasted by the model. This wind will be a function of the wavelengths and periods resolved by the model. These wavelengths are several hundreds of kilometers and the periods are greater than several hours.

Thompson (1973) demonstrated that there were two integral constraints on the essentially two dimensional synoptic scale for the atmosphere and obtained the result that the wave number spectrum varied as k^{-3} above some critical wave number, k_o, where the wavenumbers involved correspond to value like $2\pi/1000$ to $2\pi/200$ (rad/km). It is difficult, and unnecessary, to relate these wavenumbers, which begin to require global or hemispheric analysis in terms of, perhaps, some equivalent to spherical harmonics, to any corresponding frequencies.

Traditionally, however, the synoptic scale has been determined by making more or less simultaneous meteorological measurements every six hours over the Earth. There has been some effort by some meteorological centers to go to three hourly synoptic fields, especially near the surface. For some areas of the Earth, synoptic fields can be analysed on an hourly basis.

THE CLOSURE PROBLEM

Since the original work of Reynolds (1894), the study of turbulence has been carried out in a fairly standardized way. As applied to atmosperic turbulence, records of the three components of the wind are obtained of the form u(t), v(t) and w(t) as well as $T_A(t)$ (temperature) and q(t) (water vapor in the air). These records vary in duration from ten minutes, or so, to sixty minutes, depending on the available recording equipment. With T as the record duration, the quantities,

$$\bar{u} = \frac{1}{T}\int_{-T/2}^{T/2} u(t)\, dt = \langle u \rangle \tag{1}$$

$$\bar{v} = \frac{1}{T}\int_{-T/2}^{T/2} v(t)\, dt = \langle v \rangle \tag{2}$$

and so on, for the other variables are defined. These, in turn, are used to calculate

$$u'(t) = u(t) - \bar{u} \tag{3}$$

$$v'(t) = v(t) - \bar{v} \tag{4}$$

and so on. Quantities such as

$$\tau = -\rho \frac{1}{T}\int_{-T/2}^{T/2} u'(t)\, w'(t)\, dt = -\rho \langle u'\, w' \rangle \tag{5}$$

are then calculated to find the eddy fluxes of momentum, heat and water vapor. An attempt is then made to parameterize these eddy fluxes in terms of $\bar{u}$, $\bar{T}_A$ and $\bar{q}$ and their variation with elevation above a lower boundary such as the land or the ocean.

Also spectra and cross spectra are computed. A recent most important advance has been the measurement of the high frequency part of the u' spectrum and relating the spectral form in the Kolmogorov range to the flux of momentum and the calculation of τ/ρ as in the work of Large and Pond (1981).

For these microscale analyses the value of $\bar{u}$ is treated as a constant. The lowest frequency resolvable in the spectra is $n = T^{-1}$ (the averaging time). Those who make such measurements try to obtain data for conditions where $\bar{u}$ (measured in the mean wind direction) is constant for a long,long time. Rapidly varying synoptic scale conditions are frequently avoided. The notable success of these methods over the past few years more than justifies them. Nevertheless, questions on the relationships between the synoptic scale, the mesoscale, and the microscale remain unanswered.

In (1) and (2), $\bar{u}$ and $\bar{v}$ (and other quantities) are treated as a constant. Even the use of a running mean as in

$$\bar{u}\,(t) = \frac{1}{T}\int_{-T/2 + t}^{T/2 + t} u\,(\tau)\quad d\tau \tag{6}$$

and in

$$u'\,(t) = u(t) - \bar{u}(t) \tag{7}$$

meets with conceptual difficulties because, in a sense, the closure problem has been solved only for large scale conditions that cannot change with time and that are consequently inappropriate for meteorological forecasting (see Robinson (1978a). The two time series that result have had their frequency content strangely altered for example, and they represent evolutive random processes instead of stationary random processes (in the probabilistic and statistical sense). Not too much is known about the analysis of evolutive random processes.

A subtle change of definition of Eqs. (6) and (7) so as to obtain (8) and (9) has some interesting effects on the spectra. Each value of t_o produces a time series sample T minutes long for the fluctuating part referred to a single mean value instead of a continuously varying mean value.

$$\bar{u}\,(t_o) = \frac{1}{T}\int_{-t/2 + t_o}^{T/2 + t_o} u(\tau)\ d\tau \tag{8}$$

$$u'(t) = u(t) = \bar{u}(t_o)$$

$$= 0 \text{ otherwise} \qquad \text{for } -T/2 + t_o < t < T/2 + t_o \tag{9}$$

SPECTRA

Given a series of numbers, $x(m\Delta T)$ obtained every ΔT unit of time for a total time of $N\Delta T$, over the time interval $\Delta T < t < N\Delta T$, it is always possible to assume that $x(m\Delta T)$ is periodic, i.e. $x(m+pN)\Delta T) = x\ (m\Delta T)$ for any integer, p. This periodic function can then be represented by a Fourier series that will pass exactly through every value of $x(m\Delta T)$. This Fourier series will have N Fourier coefficients for the frequencies, $n = q/T$, as q varies from zero to n/2. The frequency, $n = N/2T$, is called the Nyquist frequency, or the folding frequency. Squared and averaged (or smoothed) values of the Fourier coefficients can then be interpreted as a spectrum that resolves the total variance of x(t) into frequency bands.

The frequencies involved in meteorology range over many decades on the frequency axis, corresponding to periods of millenia, centuries, decades, a year, a month, a day, hours, minutes, seconds and hundredths of a second. Examples can be found that represent many different values of both T and ΔT as defined above.

Spectra that cover three or four decades of frequency of the form, S(n) versus n, where S(n) is very large for low frequencies, are difficult to plot on linear scales. The convention, as in Van Der Hoven (1957), has been to multiply S(n) by n and graph the result on a linear vertical axis versus the logarithm of n. The resulting plot is a variance preserving plot since equation (10) holds. The spectrum has the dimensions of $x(m\Delta T)$, squared, times time.

$$\text{VAR}\ (n_2, n_1) = \int_{n_1}^{n_2} S(n)\ dn$$

$$= \int_{n_1}^{n_2} n\ S(n)\ \frac{dn}{n} \qquad (10)$$

SPECTRA THAT INCLUDE THE SYNOPTIC SCALE

Mori (1980) has made a study of the wind data at Marcus Island at the synoptic scale. He also republished five other such spectra, including the original of its kind from Van Der Hoven (1957), all graphed as n S(n) versus log n so as to be area, and hence variance, preserving.

Mori (1980) analysed the wind spectra from 10 minute averages obtained every three hours and thus introduced a substantial aliasing problem. Aliasing occurs when there are oscillations in the time history that are not reproduced when a curve is drawn through the values of, say, $x(m\Delta T)$ as plotted ΔT units of time apart. Aliasing is described in Blackman and Tukey (1958) and in Neumann and Pierson (1966). Frequencies corresponding to periods from about 20 minutes to six hours are aliased into frequencies corresponding to periods longer than six hours. The spectral graph stops abruptly at a frequency corresponding to six hours, and the value is high because of aliasing. A continuous sequence of 10 minute averages would be needed to determine the spectral content of the winds for frequencies corresponding to periods longer than 20 minutes.

Those three spectra that cover the mesoscale and microscale in the collection of Mori (1980) are suspicious in that the mesoscale and microscale parts of the spectra are impossible to interpret. Actually, the mesoscale and microscale spectra ought to be functions of the synoptic scale wind speed and of other properties of the synoptic scale that are yet to be determined.

Year long time histories sampled 100 times a second would be difficult to analyse, and the resulting spectra would be virtually useless. Smaller, properly processed, samples that still contain some information about the synoptic scale can however provide useful information about the variability of the spectra in the mesoscale range of frequencies under study.

Some spectra computed and graphed by Donelan* for various record lengths are shown in Figures 1, 2 and 3. They are all graphs of n S(n) versus log n with n in cycles per hour throughout.

---

*Personal communication

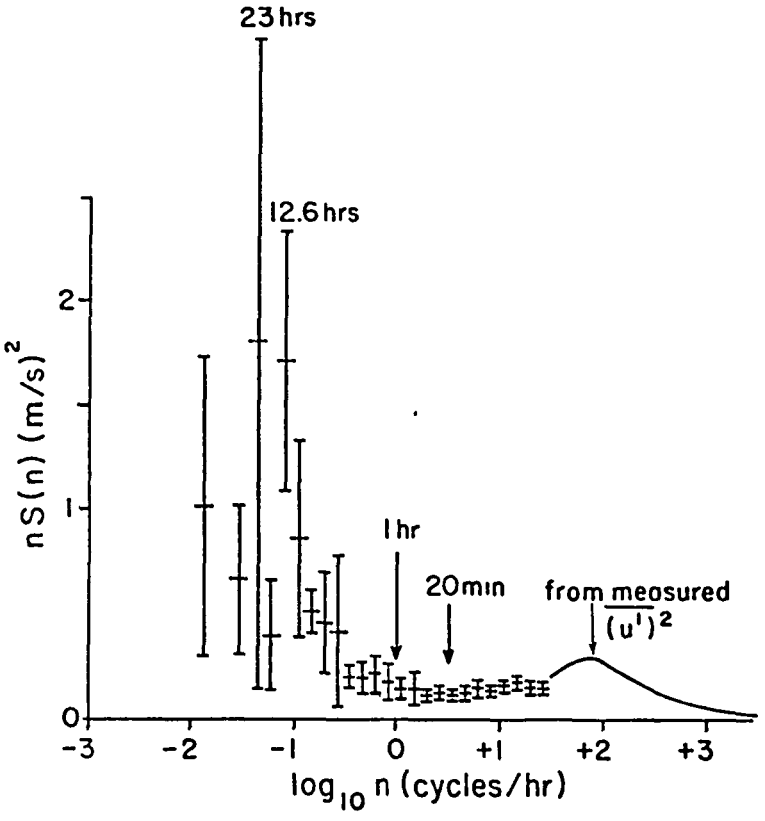

FIGURE 1 Spectrum of the wind for an average of 6.6 m/s for a 5 day, 16 hour, 32 minute sample of one minute averages combined with an estimate of the high frequency part based on measured values of u' at 5 hertz. Data from the C.C.I.W. platform with an anemometer at about 11.5 meters at Lake Ontario. (Courtesy Dr. Mark Donelan).

Figure 1 is for a 5 day, 16 hour, 32 minute (8192 minutes = 2^{13}) sample of wind speeds as one minute averages. Averaging filters out the higher frequencies, and eliminates aliasing, usually. The wind was relatively light, averaging 6.6 m/s for the 5 (plus) days. The Nyquist frequency is 30 hr^{-1} (1/120 hertz). The points represent the averages of various frequency bands, and the vertical bars represents the standard deviations of the bands that were averaged. The wind speed must have oscillated above and below the 6.6 m/s average to have produced the values in the spectrum near one half day and one day.

The smooth curve at the high frequency end is based on the analysis of a 5 sample per second subset of the data. The full spectrum shows a mesoscale valley, or flat part, that extends from a frequency corresponding to periods longer than one hour to a frequency corresponding to a period of 2 minutes.

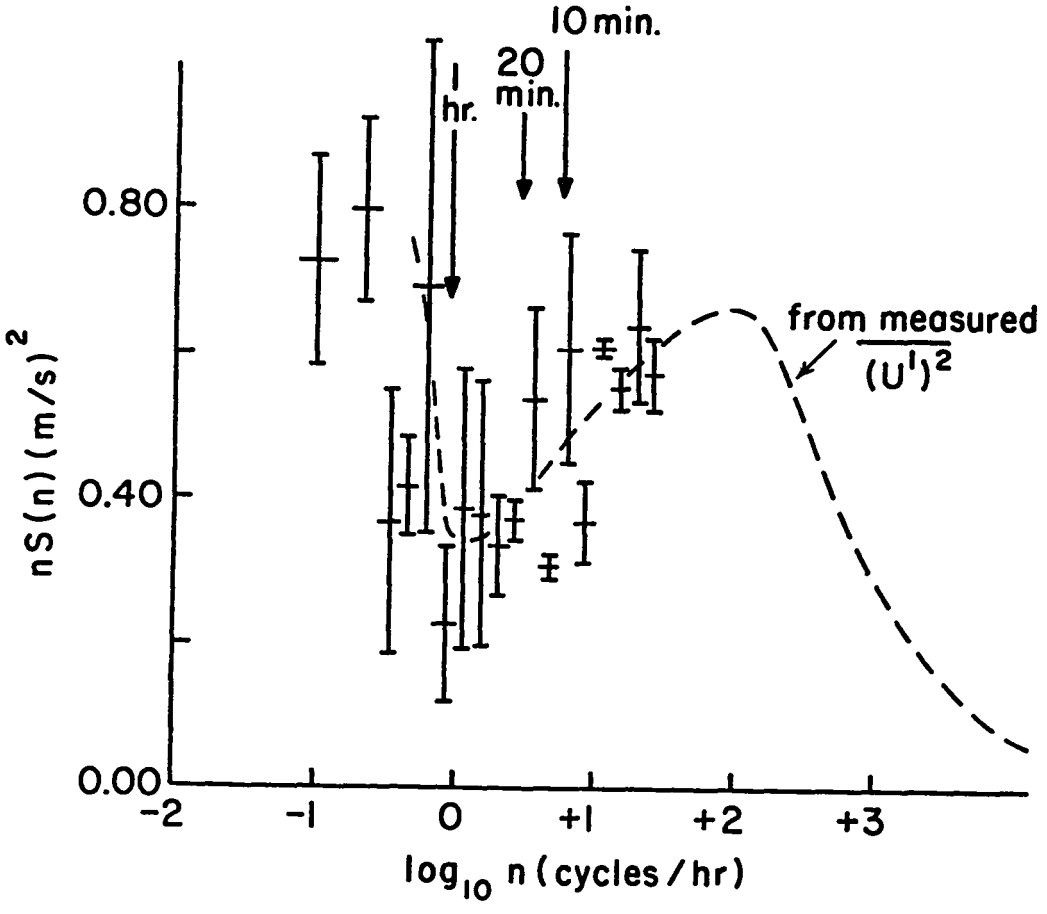

FIGURE 2 Spectrum of the wind for an average wind of 11.5 m/s for a 1 day, 1 hour, 36 minute sample of one minute averages combined with an estimate of the high frequency part based on measured values of u' at 5 hertz. Data from the C.C.I.W. platform with an anemometer at about 11.5 meters at Lake Ontario.

Figure 2 is for a mean wind of 11.5 m/s. The mesoscale valley is not as flat and as well defined, but a trace is evident between one hour and five or ten minutes. There will probably be events in the mesoscale range that cannot be explained by the present model.

Figure 3 is for 1024 one minute averages for the low frequencies combined with a high frequency spectrum computed from 5 samples per second data. The mesoscale valley exists and is moderately well defined from one hour to 5 minutes, or so.

For these three different wind speeds, there are indications that the spectral values in the mesoscale valley increase with wind speed. Also for two out of three of the spectra the values of n S(n) remain nearly constant over more than a decade of frequency range. In Figure 1, the values are more or less constant between $\log_{10} n = -0.5$ and $\log_{10} n = +1.3$, where n is in cycles per hour. These frequencies correspond to 3.16 hours (or 190 minutes) and 0.05 hours (or three minutes). In Figure 3, the values between $\log_{10} n = -0.1$ and $\log_{10} n = 1$, show some sampling variability.

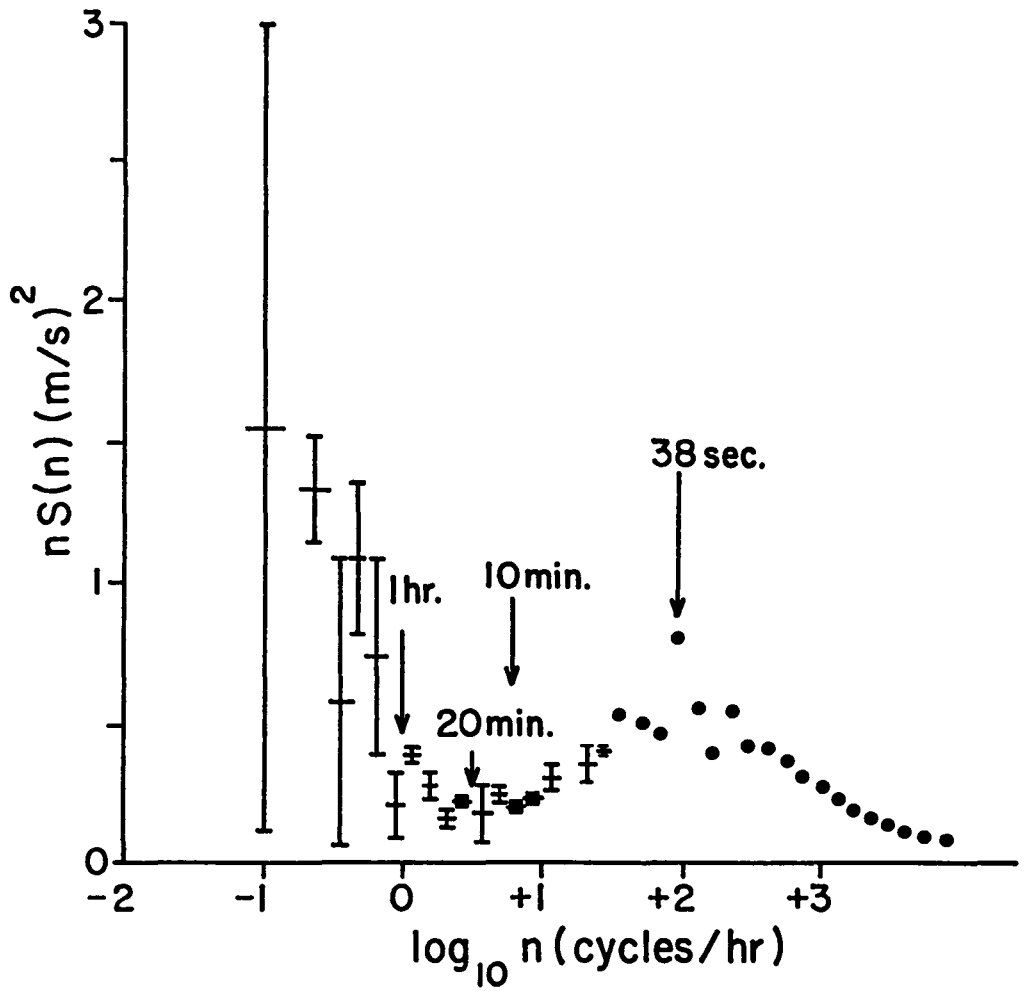

FIGURE 3 Spectrum of the wind for an average wind of 14 m/s for a 17 hour, 4 minute sample of one minute averages. Composited with an 18,000 point 5 hertz sample. Data from C.C.I.W. platform with an anemometer at about 11.5 meters at Lake Ontario. (Courtesy Dr. Mark Donelan).

Data from the North Sea provided by Dr. Klaus Hasselmann in the form of one minute averages were analysed in a different way. A time history about one month long was searched to find 256 minute (4hr 16 min) segments for which the wind speed was fairly constant. Spectra computed by the fast Fourier transform method were obtained. The component of the wind in the mean wind direction for the total sample duration was spectrally analysed. The small sample size yielded spectra that were very erratic. The spectral estimates were combined by summing over various frequency bands and by averaging over spectra with nearly the same wind speed. The circled points in the next two figures are the final results. The scales represent the relative variability of the spectral variance for the five different bands that were combined.

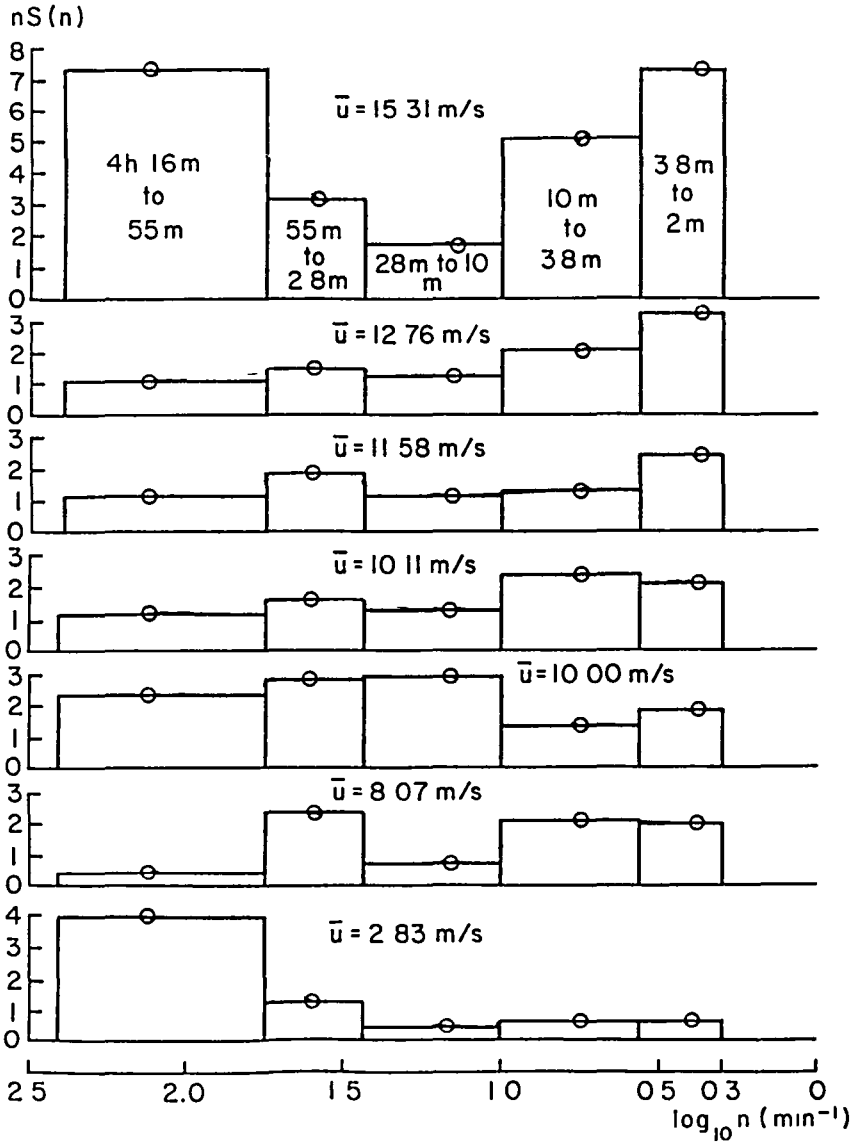

FIGURE 4 Variation of the mesoscale valley as a function of the mean wind component in the average wind direction for a 4 hour, 16 minute sample from the North Sea. The vertical scale is uncalibrated but relative changes are correct. (Data courtesy Dr. K. Hasselmann.)

Figure 4 shows results for 7 different average wind speeds. The mesoscale valley exists for all of the seven spectra. It varies in relative amplitude as both a function of frequency and wind speed. The figure has been graphed as a series of rectangular boxes to emphasize the coarseness of the frequency resolution. In all seven examples, the spectrum is fairly low to frequencies as low as those corresponding to a period of 55 minutes. For five of the seven they became even lower for still lower frequencies. The mesoscale valley may extend to low frequencies corresponding to several hours before more variable effects from the synoptic scale produce an increase in the spectrum.

When some spectra for nearly equal wind speeds are combined near 10 m/s (to stabilize the one plot for this wind speed) and the results plotted on relative scales, Figure 5 is obtained. The contribution to the variability of the wind relative to a four hour, 16 min. average in the frequency range corresponding to periods from 55 minutes to 2 minutes increases markedly with increasing wind speed. The points corresponding to the mid-points of the boxes in Figure 4 have been connected by straight lines, but the figure should still be interpreted in the same way as Figure 4.

The mesoscale range from frequencies less than those corresponding to one hour to frequencies corresponding to two minutes may actually be flat and essentially constant. The spectral estimates do not have very many degrees of freedom. Sampling variability effects are very large.

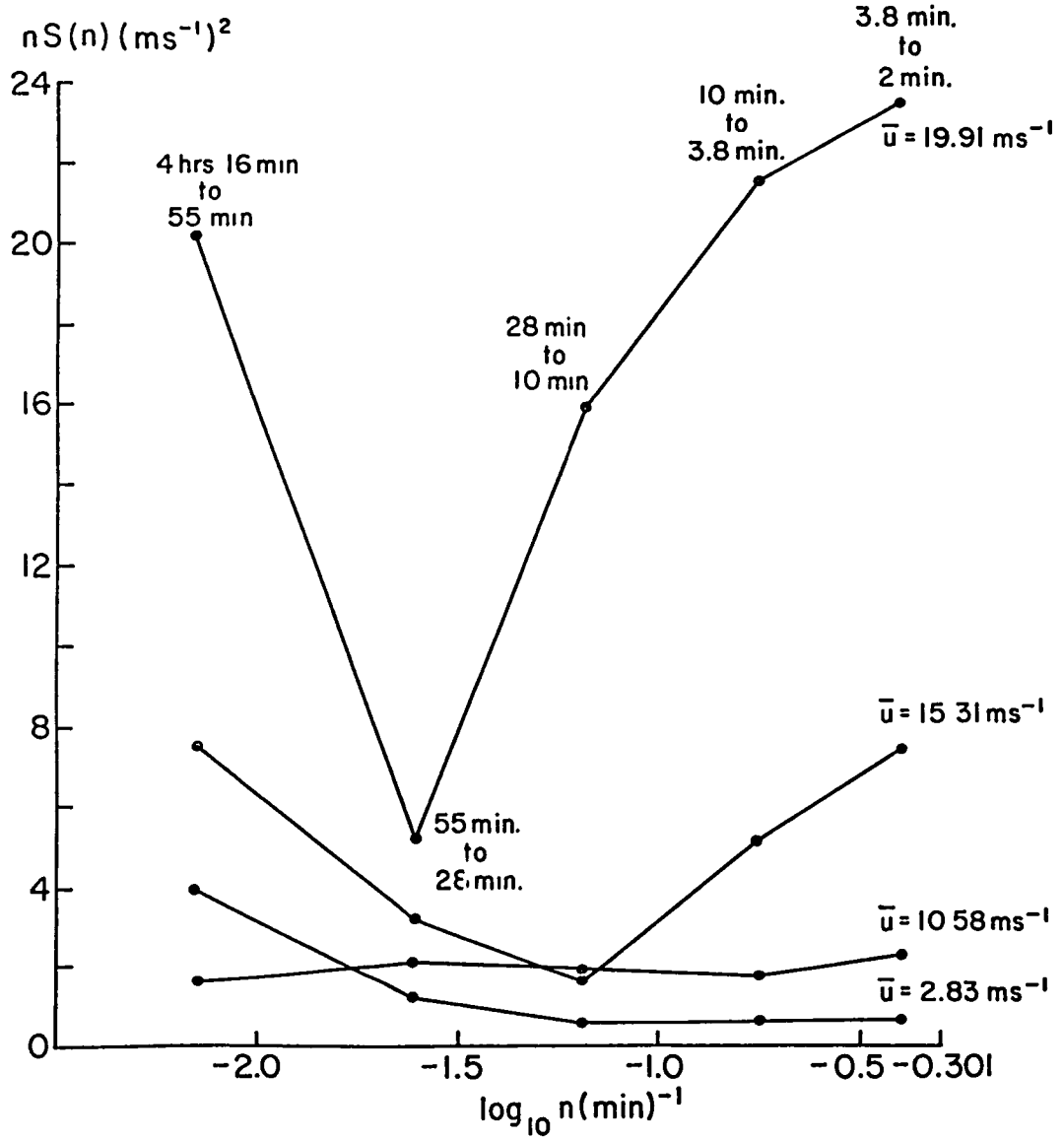

FIGURE 5 Variation of the mesoscale valley as a function of the mean wind component in the average wind direction for a 4 hour, 16 minute sample from the North Sea. The vertical scale is uncalibrated but the relative changes are correct. (Data Courtesy Dr. K. Hasselmann.)

MICROSCALE SPECTRA

Following Kaimal, et al. (1972), if equation (3) holds and if u' is spectrally analyzed in wave number space,

$$\overline{(u')^2} = \int_{k_A}^{k_B} F_u(k_1)\, dk_1 \tag{11}$$

where k_1 is a wavenumber in the u direction. From Taylor's hypothesis, if

$$k_1 = 2\pi n/\bar{u} \tag{12}$$

$$\text{then } n_A = k_A \bar{u}/2\pi, \quad n_B = k_B \bar{u}/2\pi \tag{13}$$

and

$$\overline{(\bar{u}')^2} = \int_{n_A}^{n_B} S_u(n)\, dn \tag{14}$$

where

$$\frac{2\pi}{\bar{u}} F_u\left(\frac{2\pi n}{\bar{u}}\right) = S_u(n) \tag{15}$$

and where,

$$k_1 F_u(k_1) = n S_u(n) \tag{16}$$

In wavenumber space there ought to be some range of wave numbers that follow Kolmogorov's law given by

$$F_u(k_1) = \alpha_1 \varepsilon^{2/3} k_1^{-5/3} \tag{17}$$

where α_1 is a constant (actually found from time histories) given by 0.50 ± 0.05. The quantity ε is the dissipation rate.

The basic equation for the analysis of microscale spectra in the Kolmogorov range is equation (18),

$$\frac{n S_u(n)}{u_*^2} = \frac{\alpha_1}{(2\pi\kappa)^{2/3}} \left(\frac{\kappa z \varepsilon}{u_*^3}\right)^{2/3} \left(\frac{n z}{\bar{u}}\right)^{-2/3} \tag{18}$$

where
$$\Phi_\varepsilon^{2/3} = (\kappa z \varepsilon / u_*^3)^{2/3} \tag{19}$$

and where $f = nz/\bar{u}$ (20)

The quantity in (19) can be determined by making all of the spectra go through the same point at a particular value of f. For unstable air over land (the Great Plains Experiment),

$$\Phi_\varepsilon^{2/3} = 1 + 0.5 \left| z/L \right|^{2/3} \quad \text{for} \quad -2 \leq z/L \leq 0 \tag{21a}$$

and for stable air

$$\Phi_\varepsilon^{2/3} = 1 + 2.5 \left| z/L \right|^{3/5} \quad \text{for} \quad 0 \leq z/L \leq 2 \tag{21b}$$

Equation (18) can then finally be written as (22).

$$\frac{n\, S_u(n)}{u_*^2\, \Phi_\varepsilon^{2/3}} = \frac{\alpha_1}{(2\pi\kappa)^{2/3}} f^{-2/3} \tag{22}$$

All possible turbulence spectra for the Kolmogorov inertial range ought to fall on exactly the same line when the left hand size of (22) is evaluated and plotted against f. Conversely if the spectrum is plotted as a function of f and the denominator of the right hand side is not known, the value of $u_*^2\, \Phi_\varepsilon^{2/3}$ can be computed.

Spectra of u', v', w', T' and q' have been computed for the microscale range of frequencies and plotted versus $f = n\, z/\bar{u}$ for data obtained over both the land and the ocean. The Kolmogorov range shows up in all of the spectra, but some results show differences in the low frequency form of the spectra when those obtained over land are compared to those obtained over water. McBean (1971) found spectra over land similar to the over water spectra shown below.

Figures 6 and 7 are composite plots of the spectra obtained from winds measured over land by Kaimal, et al. (1972) and over the ocean by Pond, et al. (1971), Miyake, et al. (1970) and Leavitt (1975). The continuous curves are for Kaimal, et al. (1972), who detected slightly different limit forms for neutral stability depending on whether z/L approached zero from positive or negative values in the u' and v' spectra but not for either the w' spectrum or the $u'\, w'$ co-spectrum.

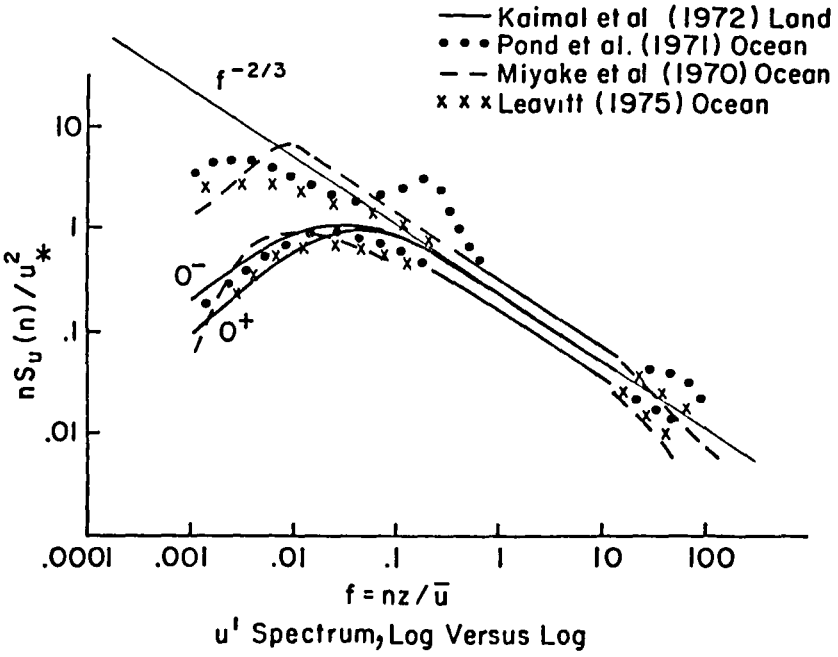

u' Spectrum, Log Versus Log

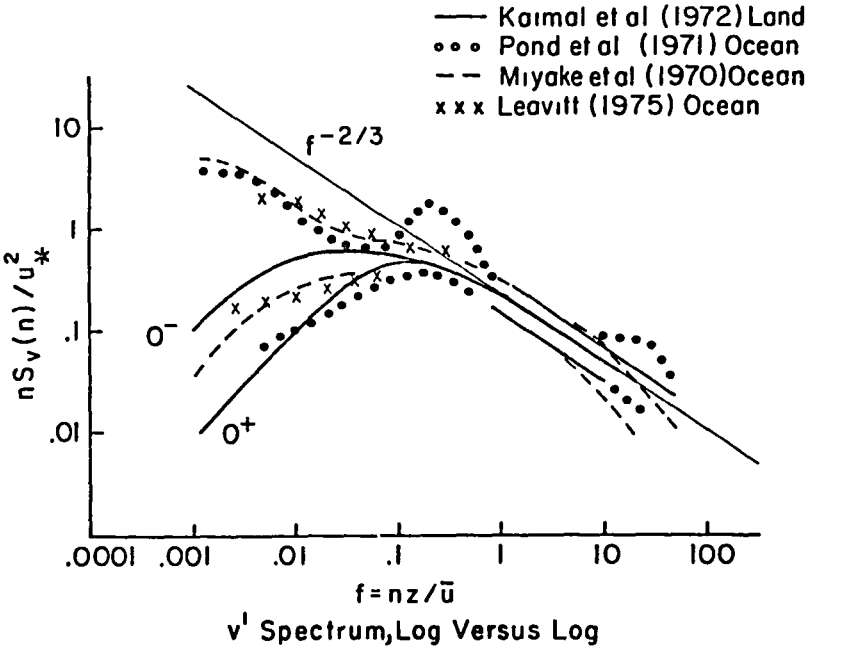

v' Spectrum, Log Versus Log

FIGURE 6 Microscale spectra for the u' and v' components of turbulence over land and the oceans.

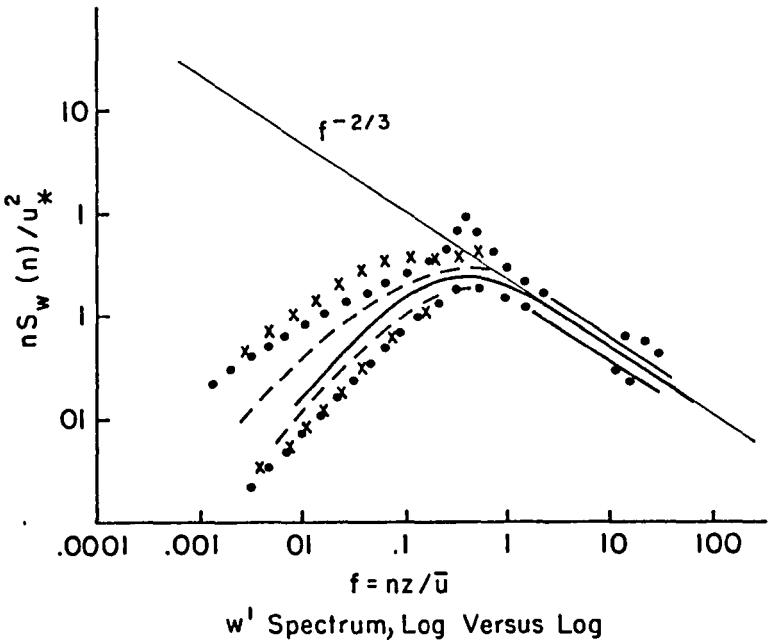

w' Spectrum, Log Versus Log

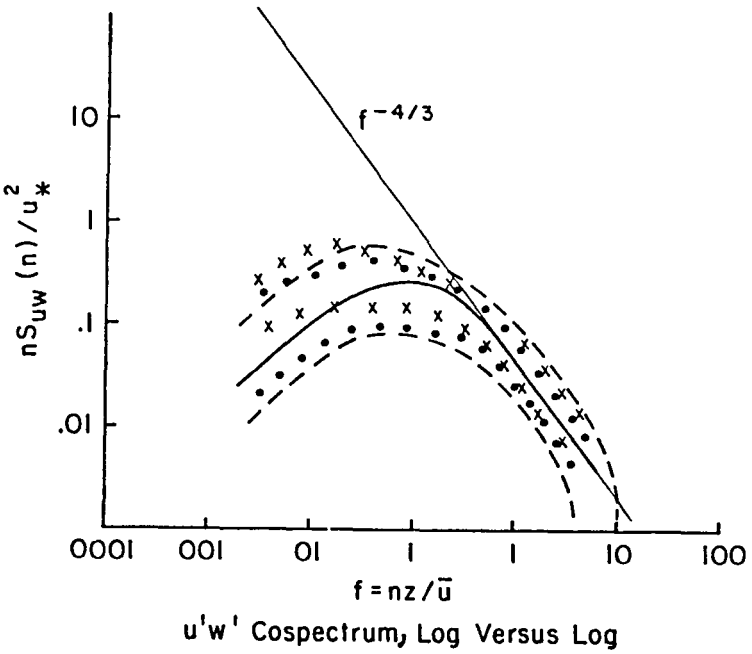

u'w' Cospectrum, Log Versus Log

FIGURE 7 Microscale spectra for w' and co-spectra for u' w' over land and over the ocean. (Coded points are the same as in Figure 6).

The coded curves show the scatter of the other three investigations for nearly neutral stability. The curves have been shifted vertically arbitrarily to match the $f^{-2/3}$ region because some of then were scaled by means of the variance of w'. The continuous curves above and below the $f^{-2/3}$ line show that the over-ocean spectra follow the minus two thirds law just as well as the one over land for u', v' and w'. At least one decade of f is spanned by the -2/3 law.

Interesting features of the u' and v' over water spectra shown in Figure 6 are that many of the spectral estimates do not decrease toward low values of f as do the over land spectra. The over land 0^+ spectra decrease by at least an order of magnitude and the 0^- spectra decrease by factor of six, or so, as f decreases from 0.03 to 0.001. At low frequencies, the over water spectra are ten to thirty times higher than the over land spectra. The spectra from Pond et al. (1971) suggest a peak somewhere near f = 0.2 to 0.3. This may be due to the motion of the platform.

In contrast, both the over land and over water spectra for w' and the cospectra for u' w' decrease with decreasing frequency. The u' w' cospectra vary as $f^{-4/3}$ for high frequencies. The u' w' cospectra obtained by Large and Pond (1981), not shown, which are plotted on a linear vertical scale, show only a minute amount of covariance below f = 0.001. The values of u_*^2 estimated from the u' w' cospectra agreed well with the bulk aerodynamic equations given by Large and Pond (1981) for 60 minute records after pooling a very large number of runs to obtain stable averages.

In terms of the mesoscale valley where n $S_u(n)$ (or n $S_{uu}(n)$) is roughly constant for frequencies corresponding to perhaps more than one hour to frequencies corresponding to several minutes, the study of micro-scale spectra has not covered a large enough frequency range.

THE SPECTRAL ANALYSIS OF MESOSCALE WIND FLUCTUATIONS

The preceding analysis has identified a frequency range in the spectra of the wind over the ocean where dominantly two dimensional turbulence-like fluctuations span about two decades of frequency for the u' and v' spectra. Just how this mesoscale range couples the synoptic scale to the microscale remains to be determined.

The dominant feature of this frequency range for the spectra is that, when the spectra are graphed in the form n S(n) versus log n, this range appears to be both flat and a minimum relative to much larger fluctuations at the synoptic scale and somewhat larger fluctuations at the microscale. The mesoscale region of the spectrum of the winds has a great deal to do with the problem of measuring the wind correctly because the frequencies involved correspond to the averaging times of 2 minutes for transient ships and 8 minutes 32 seconds for NOAA Data Buoys.

The convenience in spectral interpretation represented by a particular technique for plotting data should not be allowed to disguise the fact that the spectrum is really varying like n^{-1}. A spectral analysis of a time history with a true spectrum like n^{-1} leads to some interesting results especially at the lowest frequencies.

Consider a model of the time history of u(t) as it might be obtained for many hours as given by equation (23). The value of V can be chosen to give reasonable values for u(t).

$$u(t) = \bar{u} + \sum_i V \left(\frac{dn}{n_i}\right)^{\frac{1}{2}} (\alpha_i \cos 2\pi n_i t + \beta_i \sin 2\pi n_i t) \tag{23}$$

$$\text{for } n_1 < n_i < n_2 \tag{24}$$

where n_1 and n_2 are arbitrary.

Suppose that n varies from 10^{-6} to 10 and that over each decade there are, say, 10,000 terms in the sum. Also suppose that α_i and β_i are picked, for convenience, at random from a normal probability density function with zero mean and a unit variance and that they are all independent. For a long enough realization of this function, the distribution of values of u(t) picked at random (or at equally spaced time intervals) would be gaussian. The average as a true constant is $\bar{u}$. As defined, the function u(t) lasts forever.

Let a sample be drawn of duration T from (14), i. e. let

$$U(t) = u(t) \qquad \text{for } -T/2 + t_o < t < T/2 + t_o \tag{25}$$

This sample can be assumed to be periodic, and it can be represented by a Fourier series as in

$$U(t) = \sum_{o}^{\infty} a_m \cos \frac{2\pi mt}{T} + b_m \sin \frac{2\pi mt}{T} \tag{26}$$

The Fourier coefficients a_m are given by (27),

$$a_m = \sum_i V \left(\frac{dn}{n_i}\right)^{\frac{1}{2}} \left[\alpha_i \left[\left(\frac{\sin(\pi n_i T + \pi m)}{\pi n_i T + \pi m}\right) \cos\left((2\pi n_i + \frac{2\pi m}{T})\, t_o\right)\right.\right.$$

$$+ \left(\frac{\sin(\pi n_i T - \pi m)}{\pi n_i T - \pi m}\right) \cos\left((2\pi n_i - \frac{2\pi m}{T})\, t_o\right) \Bigg]$$

$$+ \beta_i \left[\left(\frac{\sin(\pi n_i T + \pi m)}{\pi n_i T + \pi m}\right) \sin\left((2\pi n_i + \frac{2\pi m}{T})\, t_o\right)\right.$$

$$\left.\left. + \left(\frac{\sin(\pi n_i T - \pi m)}{\pi n_i T - \pi m}\right) \sin\left(2\pi n_i - \frac{2\pi m}{T})\, t_o\right) \right] \right] \tag{27}$$

except for a_o which needs to be halved and has $\bar{u}$ added to it.

The Fourier coefficients b_m are given by a similar equation and can be obtained by interchanging sines and cosines for the terms involving t_o and by changing the three plus signs to minus signs in (27).

Usually only one sample of duration T exists to yield only one set of Fourier coefficients. The values of the Fourier coefficients are nevertheless a function of the time the sample was taken and can clearly be quite variable.

A constant term is obtained for m = 0. It is given by (28).

$$\bar{u}(t_o) = \bar{u} + \sum_i V \left(\frac{dn}{n_i}\right)^{\frac{1}{2}} \frac{\sin(\pi n_i T)}{\pi n_i T} (\alpha_i \cos 2\pi n_i t_o + \beta_i \sin 2\pi n_i t_o) \tag{28}$$

The average value of the wind thus has a spectrum. It is given by

$$\bar{S}(n) = \frac{V^2}{n} \left(\frac{\sin \pi nT}{\pi nT}\right)^2 \tag{29}$$

For a band limited n^{-1} spectrum, the values of $\bar{u}(t_o)$ will be randomly distributed with a mean of $\bar{u}$ and a variance given by the integral from n_1 to n_2 of (29).

The first harmonics, a_1 and b_1, are given by (30) and (31) at $t_o = 0$ (which is just as good a time as any other). The terms involving $\pi n_1 T + \pi$ are small. E, the expected value of the variance associated with the first harmonic, is given approximately by (32). The cross product terms add to zero in (32) and the square of the $\pi n_1 T + \pi$ term is small. The symbol E represents the expectation operator.

$$a_1 = \sum_i V \left(\frac{dn}{n_i}\right)^{\frac{1}{2}} \alpha_i \left\{ \frac{\sin(\pi n_i T - \pi)}{\pi n_i T - \pi} + \frac{\sin(\pi n_i T + \pi)}{\pi n_i T + \pi} \right\} \tag{30}$$

$$b_1 = \sum_i V \left(\frac{dn}{n_i}\right)^{\frac{1}{2}} \beta_i \left\{ \frac{\sin(\pi n_i T - \pi)}{\pi n_i T - \pi} - \frac{\sin(\pi n_i T + \pi)}{\pi n_i T + \pi} \right\} \tag{31}$$

$$E(a_1^2 + b_1^2) = \int_{n_1}^{n_2} V^2 \left(\frac{\sin(\pi nT - \pi)}{\pi nT - \pi}\right)^2 \frac{1}{n}\, dn \tag{32}$$

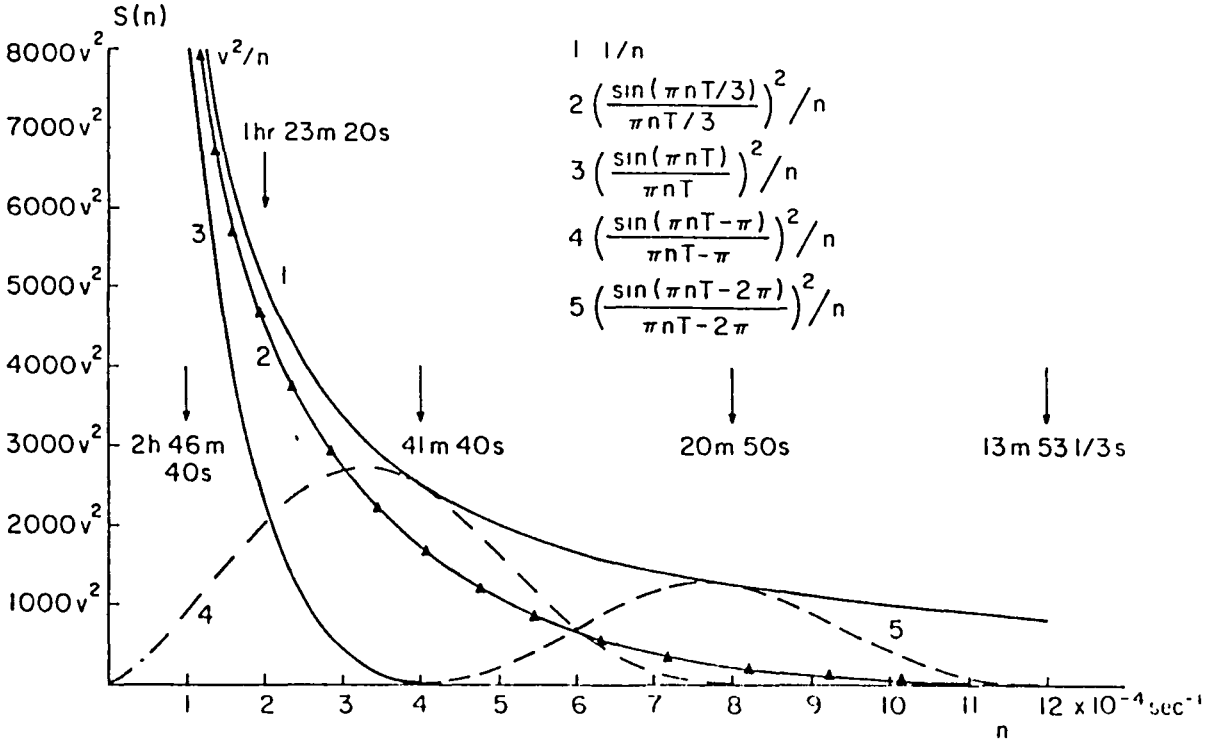

FIGURE 8. Spectra and spectral filters associated with 2500 second and 833.3 second samples and an n^{-1} spectrum.

Figure 8 is a numerical example of the equations just given. There are five curves on it. Curve 1 is the graph of $V^2\, n^{-1}$ as n varies from 10^{-4} to 12 X 10^{-4}. Curve 2 will be discussed below.

Curve 3 is the graph of equation (29) for T = 2500 seconds which corresponds to 41 minutes and 40 seconds. Curve 4 is the graph of equation (32) for the first harmonic. Curve 5 is for the second harmonic as defined on the figure. Four of the terms are of the form, $((\sin \psi)/\psi)^2$, where ψ for curve 5 (for example) is $\pi nT - 2\pi$. Beyond $\psi = \pm \pi$, the values for the function are small and the contribution outside this range can be neglected.

The first Fourier coefficient of a spectral estimate from a 2500 second sample is influenced by considerably longer periods than 2500 seconds. At least 57% of the area under the curve lies to the left of $(2500)^{-1}$ hertz.

For this model, and perhaps even for actual data, the estimate of $a_1^2 + b_1^2$ would be almost Chi Square distributed with two degrees of freedom. Even if averaged with the next two or three harmonics, this term would be so much larger than the others that its sampling variability would still dominate the average.

A paragraph from Pond, et al. (1971) is quoted below.

"In the spectra and cospectra the lower frequency points have a narrower bandwidth and hence are subject to more statistical variation. The concept of degrees of freedom which is based on Gaussian statistics in nearly useless for atmospheric turbulence data. The observed variability from block to block within a run is larger for spectra and very much larger for cospectra than the degrees of freedom concept would predict. The actual scatter in the figures is probably as good a measure as any of the statistical variability".

These spectral estimates ought to be highly variable. It is incorrect to interpret spectral estimates in terms of Gaussian statistics. Spectral estimates are Chi-Square variables. The 90% confidence interval on an approximate Chi Square with two degrees of freedom are about a factor of 60 apart.

Curve 2 in Figure 8 is the curve for the average wind except that the value of T is one third of 2500 seconds, or 13 minutes, 53 1/3 seconds. The area under curve 2 and above curve 3 represents an additional contribution to the variability of the average value of the wind that results from the briefer average.

Figure 9 shows the same five curves numbered as before and graphed with $V^2\ n\ (n^{-1})$ as the vertical scale and $\log_{10} n$ (it should really be $\ell n\ n$) as the horizontal scale. The graph rather easily covers almost two decades. The large contribution from the first harmonic is re-emphasized. The area above curve 3 and below curve 2 is clearly shown. Subsequent results are plotted in this form. but the alternate use of a plot such as Figure 8 (which is usually not feasible) must always be kept in mind as a more realistic representation of the difficulties inherent in the low frequencies.

This simple example represents an idealized mean synoptic scale wind, $\bar{u}$, perturbed by a simple mesoscale spectrum. It shows that the longer the averaging time the closer one can get to $\bar{u}$. It also shows how to compute the effect of different averaging times on the variability of the average with reference to the true average.

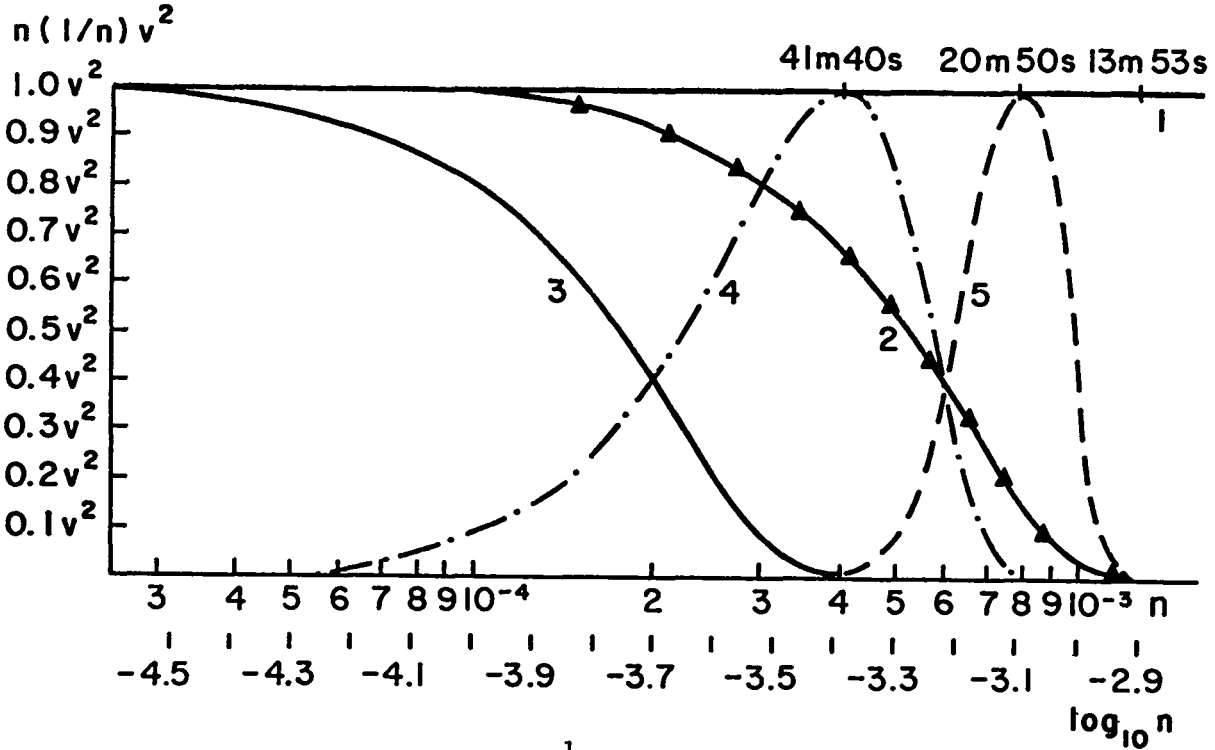

FIGURE 9 Log versus linear (n (n^{-1}) versus $\log_{10}$ n) graphs of the same curves as in Figure 8.

An advantage of this kind of plot is that the points on, say, curve 3 for the average can simply be shifted either left or right to determine the effects of any other averaging time on the value of the mean. For example, doubling the averaging time would shift the whole curve 0.3 units to the left as shown by the bottom scale.

For a spectrum given by n^{-1} there is also an equivalent square cut off frequency. If the frequency given by the averaging time is multiplied by 0.3631, a square cut off filter at this frequency will have the same area to the left (as bounded by some still lower frequency) as the $((\sin \psi)/\psi)^2$ filter. A 40 minute average is the equivalent of a 110 minute cut-off period for an n^{-1} spectrum.

MESOSCALE PLUS MICROSCALE SPECTRA

The variability of mesoscale spectra as a function of the synoptic scale mean wind can be determined from the work of Kaimal et al. (1972), Smith (1980) and Large and Pond (1981) for neutral stability. This will be done first for u' and then for v'. Then an attempt to extend the results to non zero values of z/L will be made.

For Smith (1980) and Large and Pond (1981) respectively, the typical samples were 40 and 60 minutes long. The average wind speed was calculated and various quantities were computed. Smith (1980) gives

$$\text{VAR}\,(u') = (0.061 + 0.0027\,\bar{u}_{10})^2\,\bar{u}_{10}^2 = \sigma_{u'}^2, \tag{33}$$

$$\text{and}\quad \text{VAR}\,(v') = (0.057 + 0.0017\,\bar{u}_{10})^2\,\bar{u}_{10}^2 = \sigma_{v'}^2, \tag{34}$$

and Large and Pond (1981) give

$$\text{VAR}\,(u') = (0.070 + 0.0023\,\bar{u}_{10})^2\,\bar{u}_{10}^2 \tag{35}$$

$$\text{and}\quad \text{VAR}\,(v') = (0.043 + 0.0033\,\bar{u}_{10})^2\,\bar{u}_{10}^2 \tag{36}$$

The right hand side of (22) has been expressed as a function of f even outside the range determined by the $f^{-2/3}$ law by Kaimal et al. (1972). For neutral stability since (21a) or (21b) is one, equation (22) becomes (37).

$$\frac{n\,S_u(n)}{u_*^2} = 105\,f/(1 + 33f)^{5/3} \tag{37}$$

The corresponding spectrum for v' is

$$\frac{n\,S_v(n)}{u_*^2} = 17f/(1 + 9.5f)^{5/3} \tag{38}$$

Since

$$\int_0^\infty \frac{n\,S_u(n)}{u_*^2}\,\frac{dn}{n} = \int_0^\infty \frac{105\,f}{(1 + 33f)^{5/3}}\,\frac{df}{f} = 4.77 \tag{39}$$

it follows that VAR u' for this spectrum is given by

$$\text{VAR } (u') = 4.77\ u_*^2 \tag{40}$$

Similarly $\text{VAR } (v') = 2.68\ u_*^2$ (41)

Smith (1980) gives an expression for C_{10} that allows u_* to be computed from the average wind at 10 meters. The value of u_*^2 is given by

$$u_*^2 = 10^{-3}\ (0.61 + 0.063\ \bar{u}_{10})\ \bar{u}_{10}^2 \tag{42}$$

Large and Pond (1981) give

$$u_*^2 = 10^{-3} \cdot \quad 1.2\ \bar{u}_{10}^2, \qquad \text{for } 4 \leq \bar{u}_{10} \leq 11 \text{ m/s} \tag{43}$$

$$u_*^2 = 10^{-3}\ (0.49 + 0.065\ \bar{u}_{10})\bar{u}_{10}^2 \quad \text{for } 11 \leq \bar{u}_{10} \leq 25 \text{ m/s} \tag{44}$$

Figure 10 shows graphs of equations (37) and (38) in two different forms. The upper curves are for both scales logarithmic for comparison with Figure 6. The lower curves are for a linear vertical scale so that the areas under the curves can be identified as the constants 4.77 and 2.68. Over land, according to Kaimal, et al., there is very little contribution to the u' and v' fluctuations for f less than 10^{-3}.

There are two other ways to plot the integrand of equation (37). They result from cancelling out the f in the numerator with the f in the denominator of d f/f. The function, $105\ (1+33f)^{-5/3}$, can be plotted either or linear scales for both axes or on log scales for both axes. No matter which method of plotting the spectra is used, the basic problem of what is happening at low frequencies is obscured. For what follows linear vertical scales and logarithmic horizontal scales will be used to preserve variance and to emphasise the fact that zero frequency is an unobtainable goal in meteorology.

Tables 1 and 2 give selected values of equations (33), (34), (35) (36), (37) and (38). Also shown are the differences between the variances given by (33) to (36) and (37) and (38). Over the oceans, the total variances of u' and v' are not explained by the Kaimal, et al. spectra. The unaccounted for variance at 25 m/s, for example, for u' is nearly 40% of the total variance for u' found by both Large and Pond and Smith. The corresponding standard deviations are over 1 m/s for winds over 15 m/s and over 0.5 m/s for winds over 10 m/s. There is very little difference

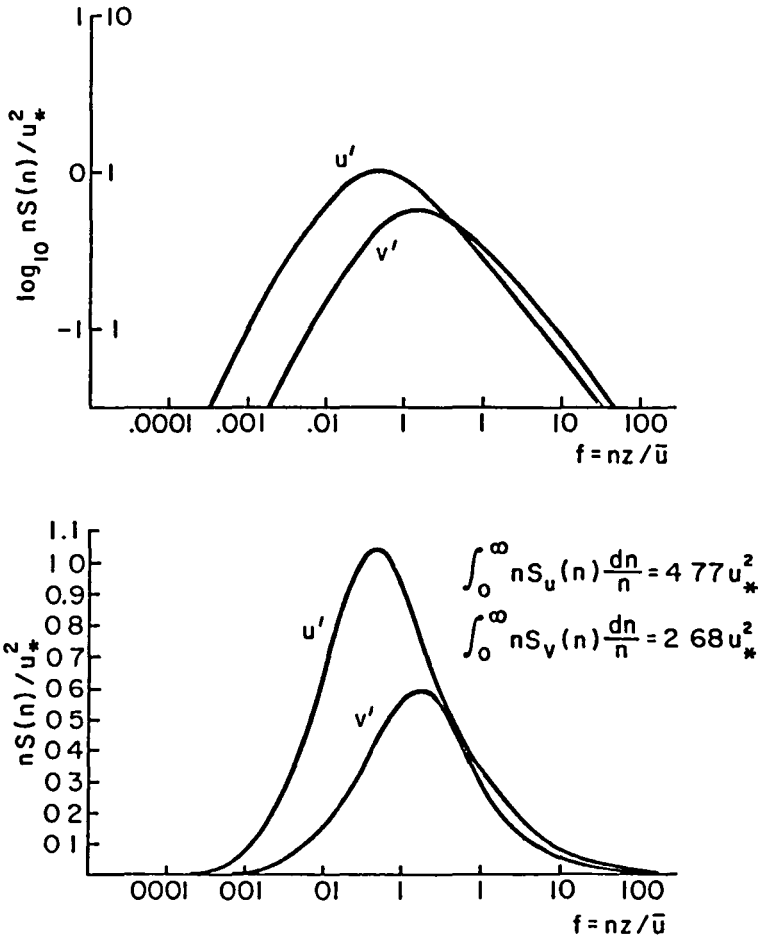

FIGURE 10 A comparison of the log versus log and log versus linear plots of the Kaimal et al. (1972) spectral forms.

between the u' and v' Kaimal et al. spectra whether computed for either Smith or Large and Pond. The VAR u' values are also essentially equal. Actually, since the Large and Pond values are for a longer averaging time, the variances ought to be larger by from 5 to 10 percent. The only major difference is that VAR v' for Smith is only about 60% of VAR v' for Large and Pond.

TABLE 1, Variances of u' as a Function of $\bar{u}_{10}$ from 40 and 60 Minute Samples Compared to the Variances Predicted by the Kaimal, et al (1972) Spectra. (Units are m/s and $(m/s)^2$)

	VARIANCE		KAIMAL, ET AL. u_* from		DIFFERENCE		CORRESPONDING STD. DEV.	
$\bar{u}_{10}$	L & P	Smith	L. & P	Smith	L. & P.	Smith	L & P.	Smith
5	0.17	0 14	0.14	0 11	0.02	0.03	0 15	0.17
7 5	0.43	0 37	0.32	0.29	0.11	0.08	0.33	0.28
10	0 86	0.77	0 57	0 59	0.27	0.18	0 54	0.43
12 5	1.52	1.40	0 70	1.04	0.55	0.36	0.74	0.60
15	2.46	2 32	1 57	1.67	0.89	0.65	0.94	0.81
17.5	3.72	3 55	2 38	2 50	1 35	1.06	1 16	1.03
20	5.38	5 29	3 42	3.57	1 96	1.72	1.40	1.31
22 5	7 51	7.51	4 71	4 88	2 79	2.62	1 67	1 62
25	10.16	10 30	6.30	6 50	3.84	3.80	1 96	1.95

TABLE 2, Variances of v' as a Function of $\bar{u}_{10}$ from 40 and 60 Minute Samples Compared to the Variances Predicted by the Kaimal, et al (1972) Spectra (Units are m/s and $(m/s)^2$).

	VARIANCE		KAIMAL, ET AL. u^* from		DIFFERENCE		CORRESPONDING STD DEV	
$\bar{u}_{10}$	L & P	Smith	L. & P	Smith	L & P	Smith	L. & P	Smith
5	0 09	0.11	0 08	0 06	0 008	0 05	0.09	0 21
7 5	0.26	0 27	0.18	0.16	0 077	0.12	0.28	0.33
10	0 58	0.55	0 32	0 33	0.25	0 21	0 51	0.46
12.5	1.11	0 96	0 55	0 59	0 56	0 37	0 75	0 61
15	1 93	1.53	0 89	0 94	1 04	0 59	1.02	0 77
17 5	3 11	2.30	1 34	1 41	1.77	0 90	1.33	0.95
20	4.75	3.31	1.92	2 01	2 83	1.30	1 68	1 14
22 5	6.96	4 58	2.65	2 75	4.31	1.83	2 08	1.35
25	9.85	6 19	3.55	3.61	5.92	2.52	2 43	1 59

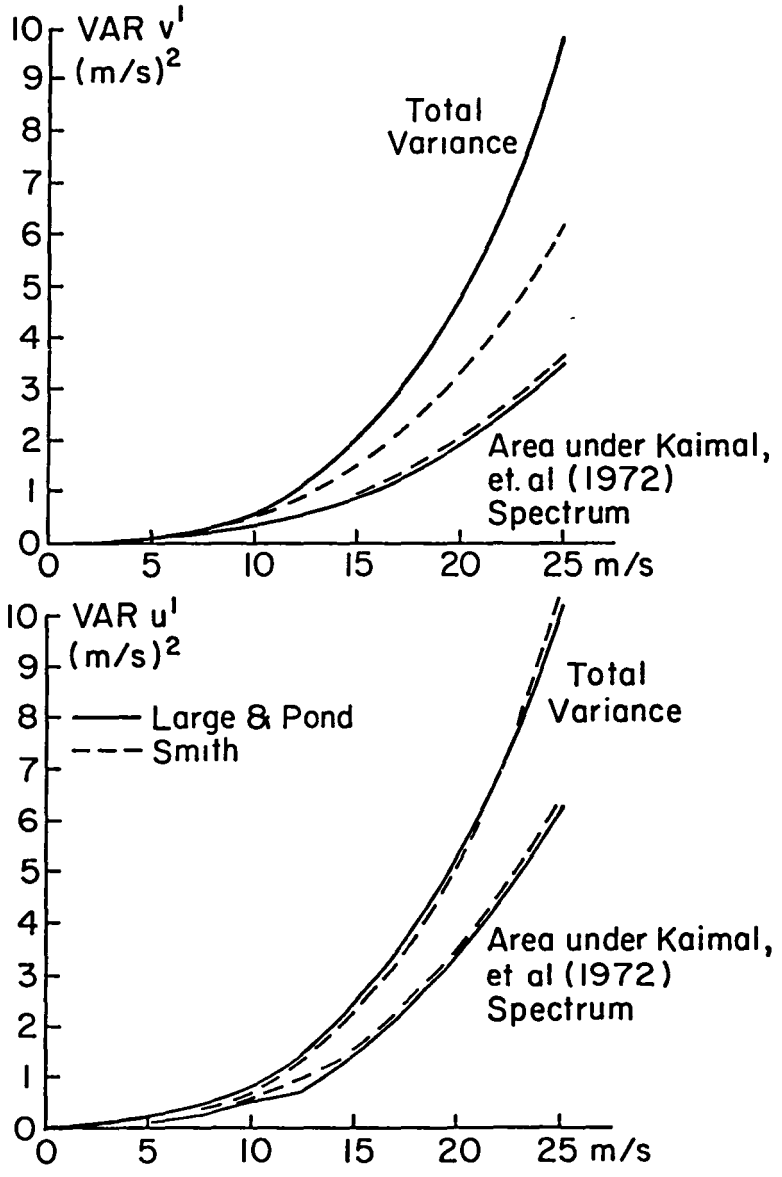

FIGURE 11 Graphs of VAR u' and VAR v' showing the amount unexplained by the microscale spectra.

Figure 11 shows graphs of the corresponding tables. For u', the total variances given by both Large and Pond and by Smith are negligably different. The areas under the Kaimal, et al. spectra predicted from two different u_*^2 equations are also negligably different for the purposes of this investigation. For v', the difference between Large and Pond and Smith for the total variance is fairly large.

If the mesoscale spectra are like n^{-1}, they should appear as a horizontal line on the bottom part of Figure 10. Suppose that the mesoscale spectrum is of the form $A\ n^{-1}$ where the unknown constant A, with the dimensions of velocity squared, is to be determined. If the right hand side of (37) is written in terms of $n = f\ z/\bar{u}$, the total variance found by, say, Smith for u' can be written as equation (45).

$$\int_{.3631/2400}^{n_I} A\ dn/n + \int_{n_I}^{\infty} (105z\ u_*^2/\bar{u}\ (1 + 33\ n\ z/\bar{u})^{5/3})dn = VAR\ (u') \tag{45}$$

This horizontal line will intersect the Kaimal, et al. spectrum at the value of n_I given by (46).

$$A = n_I\ 105z\ u_*^2/\bar{u}\ (1 + 33\ n_I\ z/\bar{u})^{5/3} \tag{46}$$

There are two unknowns and two equations. When n_I is transformed to f_I throughout in (45) and (46), there is one term involving $\bar{u}_{10}$ that does not go away.

The evaluation of the integrals and appropriate transformations yield two equations for A as a function of f_I for a fixed value of $\bar{u}_{10}$ since both u_*^2 and VAR u' are known functions of $\bar{u}_{10}$. These are equations (47) and (48).

$$A = \frac{VAR\ u' - 4.77\ u_*^2\ (1 + 33\ f_I)^{-2/3}}{\ell n\ f_I + \ell n\ \bar{u} + \ell n\ (2400/z\ (.3631))} \tag{47}$$

where z = 10 meters.

$$A = 105\ f_I\ u_*^2/(1 + 33\ f_I)^{5/3} \tag{48}$$

For particular values of $\bar{u}_{10}$, (47) and (48) can be put into the form

$$A = \frac{C_1 - C_2\ (1 + 33\ f_I)^{-2/3}}{\ell n\ f_I + C_3} \tag{49}$$

$$A = C_4\ f_I/(1 + 33\ f_I)^{5/3} \tag{50}$$

TABLE 3. Values of C_1 through C_4 and f_I based on Large and Pond (1981).

$\bar{u}_{10}$	C_1	C_2	C_3	C_3^*	C_4	f_I	f_I^*
5	0 166	0.143	8 508	8 103	3 15	0 0046	0.0055
10	0.865	0 5727	9 201	8.796	12 6	0.0117	0 0137
12	1 372	0 8728	9 384	8 979	19 2	0 0126	0 0150
15	2 457	1 573	9 607	9 202	34.61	0.0113	0.0132
20	5 382	3.417	9 894	9.489	75.18	0 0106	0.0122
25	10 16	6.309	10 118	9 713	138 8	0.0107	0.0123

The values of C_I through C_4, from the values of VAR u' and u_*^2 given by Large and Pond for a 60 minute average are shown in Table 3. Smith (1980) obtained 40 minute averages so that C_3 must be reduced by ℓn 1.5 as shown by C_3^*. Since the values for u'^3 in Table 1 are virtually identical, the actual values from Smith's equations were not used.

Equation (49) is very large for f_I slightly larger than exp $(-C_3)$, and the value of A decreases with increasing f_I. In equation (50), A increases with increasing f_I to a maximum at $f_I = 1/22$. The two curves may therefore cross at some value of f_I between exp $(-C_3)$ and 1/22. The values of f_I were found for C_3 and C_3^* and are tabulated in the last two columns of Table 3.

For $\bar{u}_{10}$ values from 10 to 25 m/s, the variation of f_I is small and so average values of 0.0114 and 0.0133 may be used. Between zero and 10 m/s, the process just used could be used to find the details of the variation of f_I (and A) with $\bar{u}_{10}$. The value of A is known directly from (50) once f_I is known. It is

$$A = 0.437\ u_*^2 \qquad \text{if } \bar{u}_{10} = 5 \text{ m/s (Smith)} \tag{51a}$$

$$A = 0.382\ u_*^2 \qquad \text{if } \bar{u}_{10} = 5 \text{ m/s (Large and Pond)} \tag{51b}$$

$$A = 0.761\ u_*^2 \qquad \text{if } 10 \leq \bar{u}_{10} \leq 25 \text{ (Smith)} \tag{51c}$$

$$A = 0.703\ u_*^2 \qquad \text{if } 10 \leq \bar{u}_{10} \leq 25 \text{ (Large and Pond)} \tag{51d}$$

It follows that the combined mesoscale-microscale spectrum of u' is given by equations (52) if equations (51a) and (51c) are used.

$$\frac{n\ S_u(n)}{u_*^2} = 0.437, \qquad f \leq 0.0055,\ \bar{u}_{10} = 5 \tag{52a}$$

and $$\frac{n\, S_u(n)}{u_*^2} = 105\, f/(1 + 33\, f)^{5/3} \qquad f \geq 0.0055,\ \bar{u}_{10} = 5 \qquad (52a)$$

$$\frac{n\, S_u(n)}{u_*^2} = 0.7614 \qquad f \leq 0.0133,\quad 10 \leq \bar{u}_{10} \leq 25 \qquad (52b)$$

and $$\frac{n\, S_u(n)}{u_*^2} = 105\, f/(1 + 33\, f)^{5/3} \qquad f \geq 0.0133,\ 10 \geq \bar{u}_{10} \geq 25 \qquad (52b)$$

These functions are graphed in Figure 12 along with some extraneous curves to help in the interpretation. The curve with triangles is the continuation of the Kaimal, et al. spectrum toward low frequencies. It is no longer needed. The dashed curve applies for 5 m/s but it not needed above 10 m/s. The dash dot curves show the effect of a 40 minute average on the full spectrum. Those for 5, 10 and 25 m/s are shown. The 10 m/s curve can be shifted to the left to the dots marked 12, 15 and 20 to find the effect of the wind speed. Just how far to the left the mesoscale spectrum extends before the sharp rise of the synoptic scale spectrum occurs cannot be determined by this particular analysis. The mesoscale, n (n^{-1}), spectrum must cover more than a decade of frequency range for $\bar{u}_{10}$ greater than 10 m/s and nearly a decade for 5 m/s.

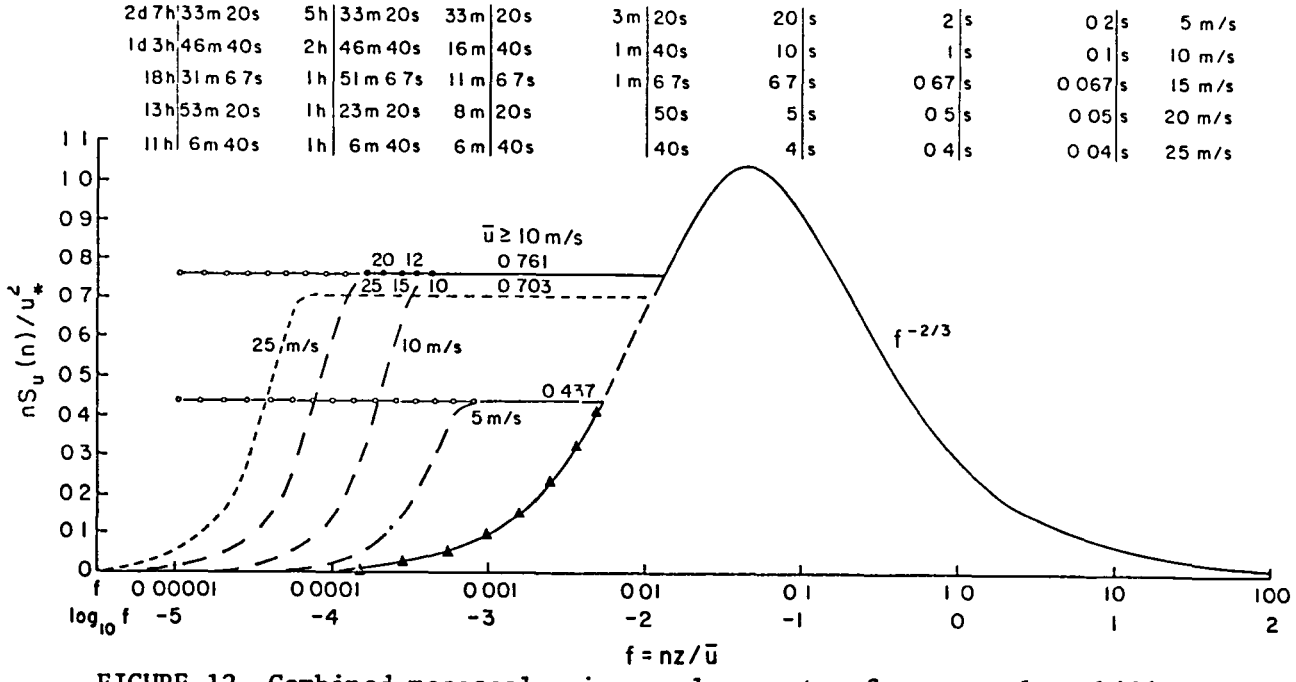

FIGURE 12 Combined mesoscale-microscale spectra for neutral stability and winds of 5 m/s and between 10 and 25 m/s.

Also shown with a different coding are the curves associated with equation (51d). The decrease in the level of the mesoscale spectrum from 0.761 to 0.703 is compensated by a shift of the spectral filter to the left to account for the longer averaging time. To obtain results based on (51b) and (51d), the standard deviations in the following tables for wind speed need only be multiplied by $(0.703/0.761)^{\frac{1}{2}} = 0.961$.

The spectra shown in Figure 12 cover seven decades of the normalized frequency (f) axis. Somewhere along the continuation of the f^{-1} part of the spectrum, an actual spectrum will rise suddenly so that synoptic scale variations can be described. The frequencies where this may happen are left undefined, and the mesoscale part of the spectrum is continued toward low frequencies by a line consisting of dashes and open circles.

A non-dimensional frequency, f, is useful in fitting the $f^{-2/3}$ region of the spectrum. For winds measured at 10 m as the mean wind speed varies from 5 to 25 m/s, the natural frequencies, n, for the full range of f in Figure 12 vary over an extensive range. The corresponding periods for these natural frequencies are shown for five different wind speeds across the top of the figure. The mesoscale periods range from about 5.5 hours to 40 seconds over about two decades on the frequency axis. At the center of the two decade range, the periods vary from 33 minutes to seven minutes. Fluctuations in the wind corresponding to these periods are essentially unpredictable at the synoptic scale. Only their statistical variability can be described as the synoptic scale evolves with time.

It is noteworthy to refer to page 721 of Smith (1980) in which the stronger increase of VAR u' than required to support the calculated drag coefficients is explained by the statement that the "same (40 min) averaging time (includes) longer turbulence length scales at higher wind speeds". The term, $\ell\eta\ \bar{u}$, in (47) accounts for this increase in the present model.

The crosswind component of the turbulent fluctuations can be analysed in terms of equations (34) and (36) and Figures 6 and 11. There are rather large differences between VAR v' as given by Large and Pond (1981) and as given by Smith (1980). There is no mesoscale spectrum that can intersect a Kaimal, et al. spectral form in a way similar to Figure 12 and give the variances of Large and Pond for high winds.

The mesoscale, v', spectrum was set equal to the maximum of equation (38), namely $0.5829\ u_*^2$, up to the non dimensional frequency of the spectral maximum, namely

$$f_{max} = 3/19 \tag{53}$$

The result is given by (54a) and (54b).

$$\frac{n\ S_v\ (n)}{u_*^2} = 0.5829 \qquad \text{for } f \leq 3/19 \tag{54a}$$

$$\frac{n\, S_v(n)}{u_*^2} = 17\, f/(1 + 9.5\, f)^{5/3} \qquad \text{for } 3/19 \leq f \tag{54b}$$

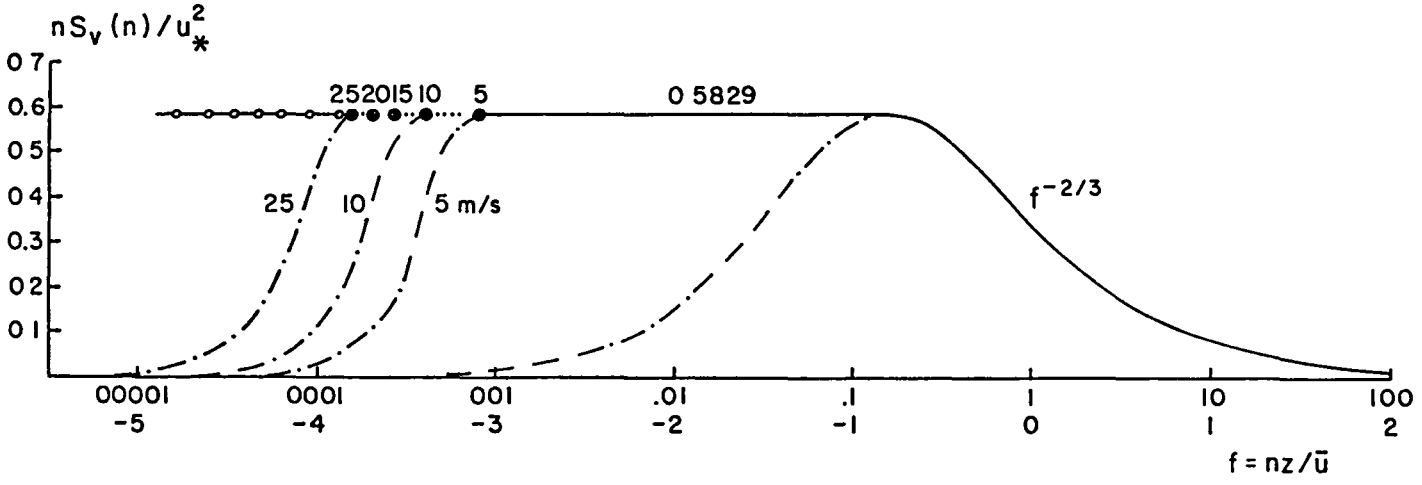

FIGURE 13 Combined mesoscale-microscale spectra for v' for neutral stability and winds from 5 to 25 m/s.

Figure 13 shows a graph of the resulting v' spectrum. Only the part past the maximum is left for the Kaimal et al. spectral form. The areas to the right of the filters labled 25, (and as interpolated 20 and 15), 10 and 5 m/s yield predictions of the variance of v' relative to a 40 minute average to determine $\bar{u}$.

With the constants for the mesoscale u' and v' spectra determined, equations similar to equation (45) can be evaluated for VAR u' and VAR v'. For example, with Large and Pond's representation for u_*^2 for $\bar{u} \geq 11$ m/s, equations (55) and (56a) can be obtained for a 40 minute average. Equation (56b) applies to the Large and Pond 60 minute average.

$$\text{VAR } u' = 10^{-3}\,(5.395 + 0.7614\ \ell n\ \bar{u})\quad (0.49 + 0.065\ \bar{u})\ \bar{u}^2 \tag{55}$$

$$\text{VAR } v' = 10^{-3}\,(4.19 + 0.5829\ \ell n\ \bar{u})\quad (0.49 + 0.065\ \bar{u})\ \bar{u}^2 \tag{56a}$$

$$\text{VAR } v' = 10^{-3}\,(4.60 + 0.5829\ \ell n\ \bar{u})\quad (0.49 + 0.065\ \bar{u})\ \bar{u}^2 \tag{56b}$$

Similar equations for the other ranges of wind speed and for the values of u_*^2 predicted by Smith can also be obtained. Values from these equations for 2.5 m/s increments in wind speed are given in Tables 4 and 5. The different models are all quite close together for the u' variability except that the spectral model yields standard deviations about 20 cm/sec too high for high winds as would be expected from Table 3.

TABLE 4; Variances and Standard Deviations of u' Relative to a 40 Minute Average Wind Computed for Various Models

	VARIANCE			STANDARD DEVIATION		
$\bar{u}_{10}$	L & P	Smith	This Model u_*(L & P)	L & P	Smith	This Model u_*(L & P)
5	0.17	0.14	0 17	0.41	0.37	0.41
7 5	0.43	0.37	UNDEF	0.66	0.61	UNDEF
10	0.86	0.77	0.86	0.93	0.88	0 93
12.5	1.52	1 40	1.49	1.23	1.18	1.22
15	2.46	2.32	2.46	1.57	1 52	1.57
17.5	3.72	3.55	3 78	1.93	1.88	1.94
20	5.38	5.29	6.01	2.32	2.30	2.45
22.5	7.51	7.51	8 41	2.74	2.74	2.90
25	10.16	10 30	11.39	3.19	3.21	3.37

TABLE 5; Variances and Standard Deviations of v' Relative to 40 and 60 Minute Average Winds Computed for Various Models.

	VARIANCE				STANDARD DEVIATION			
			This Model				This Model	
$\bar{u}_{10}$	L. & P. (60)	Smith (40)	L. & P (60)	Smith (40)	L. & P. (60)	Smith (40)	L. & P. (60)	Smith (40)
5	0.09	0 11	0.16	0.13	0.30	0 33	0.40	0.36
7.5	0 26	0.27	0.39	0.29	0.51	0 52	0.62	0.54
10	0 58	0.55	0.71	0.69	0 76	0 74	0.84	0.83
12.5	1.11	0.96	1 23	1 24	1 05	0.98	1.11	1.11
15	1.93	1.53	2 05	2.02	1 39	1.24	1.43	1.42
17.5	3.11	2 30	3.12	3.07	1.76	1.52	1.77	1.75
20	4.75	3.31	4.56	4.40	2 18	1.82	2.14	2.10
22.5	6.96	4.58	6.35	6.16	2.64	2.14	2.52	2.48
25	9.85	6.19	8.55	8.33	3.14	2 49	2.92	2.89

The two different representations for VAR v' cannot both be fitted by one model. The model used is closer to the results of Large and Pond. The standard deviations are somewhat high for light winds, and the combined mesoscale microscale spectrum may have a slight peak.

The effect of atmospheric stability on the mesoscale-microscale spectrum for winds over the ocean is difficult to determine because most of the studies have concentrated on near neutral conditions. Kaimal et al. (1972) show spectra for u' and v' as z/L, where L is the Monin-Obukov stability length and z is 10 meters, varies from -2.00 to + 2.00 for data obtained over land. There do not appear to be corresponding spectra for over water conditions.

Leavitt (1975) has reported some data for a z/L value over the tropical ocean of -1.26. Large (1979) has tabulated much of the data used in Large and Pond (1981). The highest z/L value in the tabulation is + 0.3 for an air-sea temperature difference of + 5.6° C. The lowest value is -0.45 for an air-sea temperature difference of -17.3° C. These extremes are typical of ship reports in mid-latitudes. Values of z/L between -1.00 and + 0.50 are probably representative of most over ocean conditions.

In order to obtain some idea of the effects of stability on the variability of mesoscale wind fluctuations, the mesoscale portion has been scaled according to $u_*^2 \ \Phi_\varepsilon^{2/3}$ (see, equations 21a and 21b), and an empirical fit has been made to the microscale spectra graphed in Figure 5 (not shown) of Kaimal, et al. (1972). Equation (57) is for $z/L < 0$, and equation (58) is for $z/L > 0$. To simplify matters only winds greater than 10 m/s will be considered.

For $-2 \leq z/L \leq 0$, $\qquad 10 \leq \bar{u}_{10} \leq 25$

$$\frac{n\, S_u(n)}{u_*^2 \ \Phi_\varepsilon^{2/3}} = 0.7614 \qquad \text{for } f \leq f_I \tag{57a}$$

$$\frac{n\, S_u(n)}{u_*^2 \ \Phi_\varepsilon^{2/3}} = 0.0303 \ \frac{(1 + 33\ (1 + 1.77\ |\ z/L\ |)\ 4)^{5/3}\ f}{(1 + 33\ (1 + 1.77\ |\ z/L\ |)f)^{5/3}}$$

$$\text{for } f_I \geq f \tag{57b}$$

For $0 \leq z/L \leq 0.8$, $\qquad 10 \leq \bar{u}_{10} \leq 25$

$$\frac{n\, S_u(n)}{u_*^2 \ \Phi_\varepsilon^{2/3}} = 0.7614 \qquad \text{for } f \leq f_I \tag{58a}$$

$$\frac{n\, S_u(n)}{u_*^2\ \Phi_\varepsilon^{2/3}} = 0.0303\ \frac{(1 + 33\ (1 - 0.443\ |\ z/L|)4)^{5/3}\ f}{(1 + 33\ (1 - 0.443\ |\ z/L|)\ f)^{5/3}}$$

$$f_I \geq f \qquad (58b)$$

Both (57b) and (58b) reduce to (52) at z/L equal to zero. Figure 14a shows (57b) and (58b) graphed for different z/L values on logarithmic scales for both axes for comparison to the original figure. Fig. (14b) shows the same functions graphed for a linear vertical scale and a logarithmic horizontal scale. An interesting feature of the empirical fit is the rapid change as z/L varies from zero to -0.5 which may be related to the excluded region of Kaimal, et al.

Equations (57b) and (58b) can easily be integrated to find the area under the spectrum. These values are tabulated on the figure as a function of z/L. The area increases by a factor of 10. As z/L decreases toward -2.00, the denominator of the left hand side of (57b) increases more strongly than u_*^2 so that the combined effect of the increasing area under the normalized spectrum and the increasing normalizing term will result in high values of VAR u'. As z/L increases toward +2.00, the denominator of the left hand side of (58b) increases more strongly than u_*^2 which compensates in part for the decreasing area under the normalized spectrum.

The mesoscale part of the spectrum is shown on Figure 14b as a dashed horizontal line at the value 0.7614. The non-dimensional frequency, f_I, at which the mesoscale spectrum intersects the Kaimal-type spectrum can be read from the figure for various z/L values. These are tabulated below. For z/L greater than about +0.8, there is no intersection. Perhaps the combined spectra resemble Figure 13 as has been assumed for Table 6. From Figure 12, to locate the lower limit of integration, a 40 minute average and VAR u' relative to a 40 minute average would involve very little of the mesoscale part of the spectrum for highly unstable air.

TABLE 6; Values of f_I and the "Mesoscale Constant" as a Function of z/L from Figure 14b.

z/L	$\mathrm{Log}_{10}\ f_I$	f_I	Mesoscale Constant
-2.0	-3.13	0.00074	0.7614
-1.5	-2.98	0.00105	0.7614
-1.0	-2.77	0.00170	0.7614
-0.5	-2.44	0.00363	0.7614
-0	-1.88	0.0133	0.7614
+0.5	-1.62	0.0240	0.7614
+1.0	-1.1	0.0794	0.72
+1.5	-0.85	0.141	0.52
+2.0	-0.45	0.355	0.26

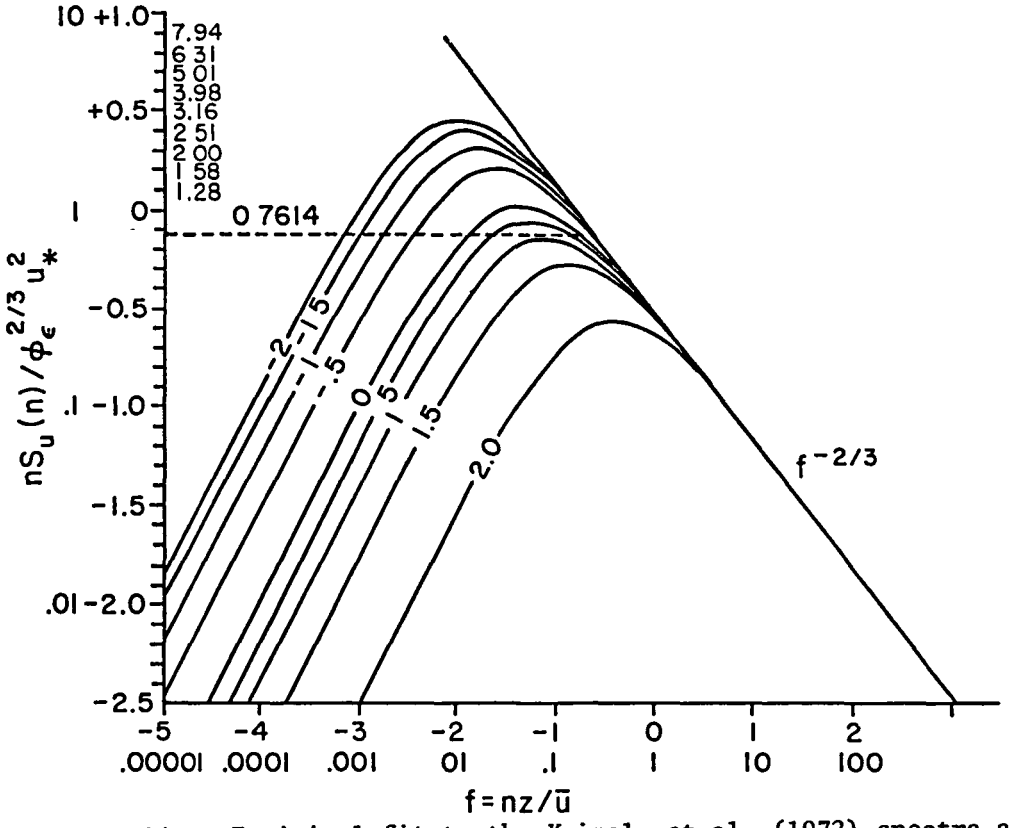

FIGURE 14a Empirical fit to the Kaimal, et al. (1972) spectra as a function of z/L plus the mesoscale spectrum for z/L less then 0.8 (log versus log). Each scale is labelled in two ways: log and dimensional.

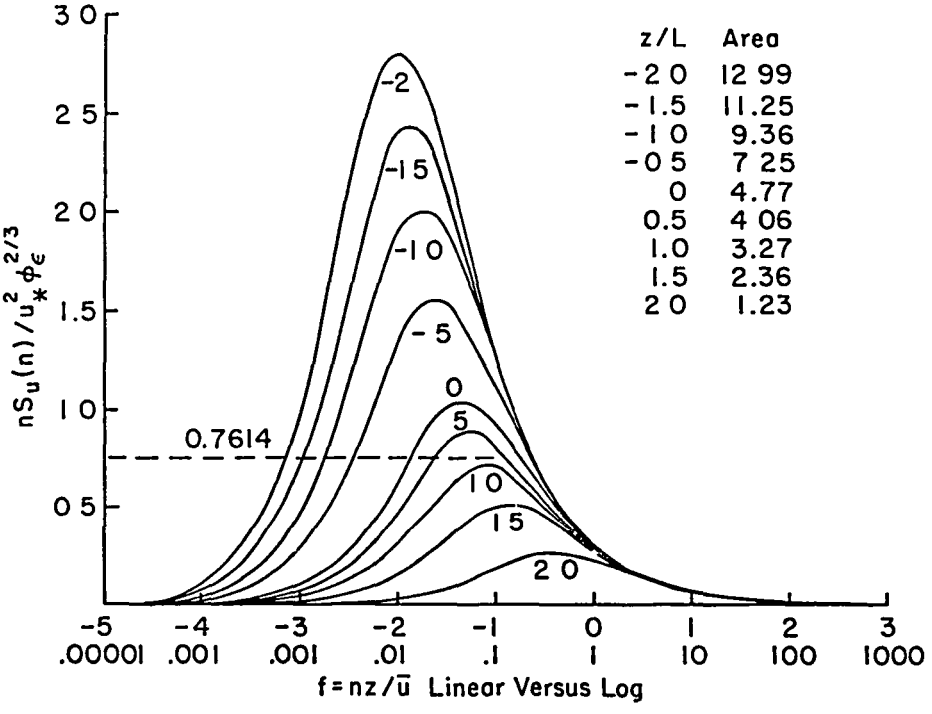

FIGURE 14b Empirical fit to Kaimal, et al. (1972) spectra as in Fig. 14a (log versus linear).

The above assumed scaling for the mesoscale part of the spectrum requires verification. Figure 14b suggests that VAR u' can be two or three times greater for an unstably stratified atmosphere for the same wind stress than it is for a neutral atmosphere.

A corresponding highly speculative spectrum for v' for the combined mesoscale-microscale range is given by equations (59) and (60).

For $-2 \leq z/L \leq 0$, $\quad 10 \leq \bar{u}_{10} \leq 25$

$$\frac{n\, S_v(n)}{u_*^2\, \Phi_\epsilon^{2/3}} = 0.5829 \qquad \text{for } f \leq f_I \tag{59a}$$

$$\frac{n\, S_v(n)}{u_*^2\, \Phi_\epsilon^{2/3}} = 0.0379\, \frac{(1 + 9.5\,(1 + 1.77\,|\,z/L\,|)4)^{5/3}\, f}{(1 + 9.5\,(1 + 1.77\,|\,z/L\,|)f)^{5/3}} = G(f)$$

$$\text{for } f_I \leq f \tag{59b}$$

For $0 \leq z/L \leq 2$, $\quad 10 \leq \bar{u}_{10} \leq 25$

$$\frac{n\, S_v(n)}{u_*^2\, \Phi_\epsilon^{2/3}} = G^*(f_{max}) \qquad \text{for } f < f_{max} \tag{60a}$$

$$\frac{n\, S_v(n)}{u_*^2\, \Phi_\epsilon^{2/3}} = G^*(f) \qquad \text{for } f_{max} < f \tag{60b}$$

where $G^*(f)$ is defined from (59b) by substituting -0.443 for + 1.77.

For unstable stratification, the spectra resemble Figures 12 and 14. For stable stratification, they resemble the spectra assumed for z/L greater than 0.8. These forms also require further verification.

There are other ways that the spectra could depend on atmospheric stability. As one example, the ratio of the spectral peak for z/L equal to zero to the value, 0.7614 is some constant. As z/L varies, this constant ratio could be maintained, and the mesoscale spectrum would then increase and decrease even more strongly as a function of z/L. The quantities VAR u' and VAR v' would then be very strongly dependent on z/L as well as on u_*^2.

All of these model spectra are asymptotic to $f^{-2/3}$ at high non-dimensional frequencies.

They all fit equation (22) for the same α_1 for u'. At still higher non-dimensional frequencies they must decrease even more strongly so as to describe properly the true molecular dissipation range as in Gibson (1963).

The spectra that have been derived depend on $\bar{u}$, via $f = n\ z/\bar{u}$ where z is 10 meters, on u_* and on z/L evaluated at 10 meters. The roughness length z_o is a function of u_* and not of L, which, is the Monin-Obukov length.

As given, for example, in Large and Pond (1981),

$$U(z) = (u_*/\kappa)\ [\ell n\ (z/z_o) - \psi(z/L)\ ] \qquad (61)$$

If $\psi(z/L)$ is zero and if $u_*^2 = C_{D10}\ U_{10}^2$ is known, then z_o is uniquely determined. For z/L non zero, and a given u_*, equation (61) can be written as equation (62).

$$U(z) = U_{neutral}\ (z,\ u_*) - \frac{u_*}{\kappa}\ \psi\ (z/L) \qquad (62)$$

The wind at 10 meters will therefore be either stronger or weaker in a stratified atmosphere for a fixed u_* as a function of z/L. In principle this wind, at least according to equation (15), should be used to recover the natural frequencies in the spectrum.

The wind speeds at ten meters for given values of u_* and z/L are given in Table 7. The form for $\psi(z/L)$ given by Large and Pond has been used. Under unstable conditions, a much lighter wind is required to produce the same stress at the sea surface than for neutral conditions, and conversely for stable conditions. By interpolation in Table 7, the values of u_* for wind speeds measured at 10 meters as z/L is varied are given in Table 8. As an example, a wind of 25 m/s at 10 meters for z/L = -1, can exert a stress that is 3.5 times greater than a 20 m/s wind for z/L = +0.5. The tables indicate that a variation of z/L from -1.00 to +0.5 is sufficient to represent most over ocean conditions. Values of z/L of +0.5 associated with winds at 10 meters of 20 m/s or higher would be found only in the warm sectors of intense extratropical non-occluded cyclones.

The spectra in Figure 12, 13, and 14 and the v' spectra defined by (61) and (62) can be thought of in an interesting way. The synoptic scale spectrum is generated over days, weeks and months. In terms of the synoptic wind field it must at a minimum be represented by two wavenumbers (combined as the magnitude of the vector wavenumber) in the horizontal direction and a frequency. At a given point near the ocean surface, for times of the order of several hours, there will exist, because of the synoptic patterns, a nearly constant wind speed and direction at 10 m above the sea surface. These mesoscale-microscale spectra can then be found for that wind speed.

They represent the eddy fluctuations about the mean wind in the direction of the mean wind speed and the eddy fluctuations transverse to the mean wind. As the synoptic scale wind speed and the value of z/L change "slowly" the mesoscale-microscale spectra will change as a function of the mean wind and the stability.

TABLE 7; $\bar{U}_{10}$(m/s) As a Function of u_*(m/s) and z/L at 10 Meters.

z/L	-1	-0.5	0	+0.5
ψ(z/L)	1.248	0.789	0	-2.5
u_* (m/s)				
0.173	4.47	4.67	5	6.05
0.346	8.95	9.33	10	12.11
0.451	11.13	11.63	12.5	15.25
0.571	13.26	13.90	15	20.98
0.706	15.35	16.14	17.5	24.30
0.846	17.42	18.37	20	25.16
0.994	19.47	20.59	22.5	28.56
1.149	21.50	22.79	25	32.01
1.312	23.50	24.97	27.5	35.50
1.482	25.48	27.15	30	39.03

TABLE 8: u_*(m/s) As a Function of $\bar{U}_{10}$ and z/L at 10 Meters.

z/L	-1	-0.5	0	+0.5
$\bar{U}_{10}$(m/s)				
5	0.192	0.185	0.173	0.143
10	0.397	0.377	0.346	0.285
12.5	0.528	0.497	0.451	0.359
15	0.692	0.637	0.571	0.443
17.5	0.852	0.791	0.706	0.498
20	1.034	0.955	0.846	0.550
22.5	1.231	1.129	0.994	0.633
25	1.441	1.314	1.149	0.820

DATA BUOYS AND TRANSIENT SHIPS

The winds near the surface of the ocean are presently measured by anemometers on anchored data buoys and by transient ships of opportunity. Other ships still report Beaufort estimates of the winds, which are better than nothing at all, but not much. These winds combined with the other data that are reported are the basis for the analysis of the synoptic fields for the lower layers of the atmosphere required for a computer based numerical weather prediction. There are many uses for these wind measurements, but the most important use is for the initial value specification of a synoptic scale forecast. If the winds are measured correctly for this particular use, all other uses will be equally well satisfied (and even better satisfied).

In addition to the problem of determining the proper averaging times for synoptic scale winds, there is the equally difficult problem of the calibration and exposure of anemometers on ships and data buoys because of their different locations and designs. The analysis in this paper avoids the very complex question of anemometer exposure from one ship to another and the problem of properly calibrating the anemometer because of its particular location on a particular ship.

Examples of this kind of problem are illustrated by the papers by Augstein, et al. (1974) and Kidwell and Seguin (1978). Augstein, et al. (1974) compared winds measured by the anemometer on the "Meteor" with winds measured by the meteorological buoy of Hamburg University. From the data, one suspects that the air flow over the bridge created a volume of quasi-stagnation behind and over it such that for high winds the "Meteor" winds dropped by 3 or 4 m/s compared to those measured by the buoy.

Similarly Kidwell and Seguin (1978) compared mast and boom anemometer measurements for four different ships in the same "synoptic" wind field equipped with identical instrumentation during GATE. The lack of agreement was substantial and beyond the scope of this particular paper.

These two reports are mentioned solely to point out the difficulties associated with ship reports. These problems need solutions as well as the problem of properly measuring the synoptic scale wind given "errorless" measurement systems.

The great success of the Seasat-JASIN program (Jones et al. (1982), Brown et al. (1982) and Schroeder et al. (1982)) is due to the careful cross calibration of all of the anemometers that were used, as described in Businger et al. (1980).

The weather ships of the past four decades or so are being withdrawn from service. Data from these ships have been invaluable in many scientific programs, and I wish to acknowledge the contributions of the officers and men who provided data from India, Juliet, Kilo and Papa during Skylab and from Papa during Seasat.

Their place is being taken by data buoys, which have been placed in operation by many different nations. In this section, ways to improve the measurement of the wind with these data buoys will be described first. This will be followed by the treatment of ways to improve measurements by ships.

When the United States NOAA Data Buoy System was in the planning and design stage, studies were made of optimum design and measurement procedures. Spectra for a limited number of oceanic sites similar to some of those of Mori (1980) were presented. These all showed a mesoscale valley, and there was no aliasing. Different methods for averaging the winds were considered.

A report by Adamo, et al. (1971) recommended averaging times longer than one hour and demonstrated a minimum environmental error for this averaging time. Much longer averaging times very rapidly involved the synoptic scale and the environmental error rapidly increased. Too long an averaging time will begin to remove some of the synoptic scale information from the winds.

The final report for the program was by Baer, et al. (1972). In a summary by R. W. Severance and L. Baer, a sequence of three 20 minute samples is recommended, that could in turn have been averaged to obtain a one hour average wind.

One could consider a much wider range of possible averaging times for anemometer records starting with, say 12 hours and ending with one second, for example. Each would yield a vector wind. This vector wind could be compared to that vector wind that ought to have been obtained for use in a synoptic scale model either for verification or initialization purposes. For most parts of the world a 12 hour wind average would be quite different from the desired value and produce a large error. A one second average would be equally poor for a different reason. For minimum "error", or for a minimum value of the standard deviation of the average value relative to the synoptic value at some fixed location, there must be some averaging time that would be optimum. The graph of standard deviation versus averaging time would be shaped like the letter "U" or perhaps like a longitudinal section through the center line of a bathtub. Thus, when this problem was first brought up in connection with measuring winds with the scatterometer on Seasat, it was promptly identified by the scientists at NASA Langley as the "bathtub" problem.

In concept, at least, the bottom of the bathtub for error free instrumentation might correspond to a point with zero standard deviation. However,one might suspect that different synoptic scale patterns and different locations in such a pattern would require different averaging times. A one hour average during a frontal passage might not be the appropriate thing to do.

Two NOAA Data Buoys recently anchored off California have been modified to provide wind data that is different from that previously obtained. These buoys report 58 minute wind averages each hour as well as 8.5 minute averages.

The highest 8 second gusts during both the 8.5 and the 58 minute averages are also given. Two minutes are lost each hour so that the data can be transmitted.

Figures 15 and 16 are the most detailed. The bottom part shows wind speed, and the top part shows direction. The continuous jagged line connects the points each hour for the 58 minute averages. The X's are 8.5 minute averages obtained once during each of the 58 minute averages. The black dots are the 8 second gusts for the 8.5 minute average, and the open circles are the 8 second gusts for the 58 minute average. Individual gusts exceed the 58 minute average winds by 6.5 to 7 m/s. The line for the 58 minute averages is usually, but not always, smoother than a line connecting the 8.5 minute averages would be. A synoptic scale, hour by hour, prediction of the wind at these two locations would probably produce even smoother curves than the ones for the 58 minute averages. The 8.5 minute mesoscale variability is particularly noticeable for Figure 15 on Dec. 3 from 1200 to 1800.

After 0100 Dec. 4 in Figure 15, the wind speed decreases from 15 m/s to 7.2 m/s in 3 hours. Both the 58 minute and 8.5 minute averages track the decrease equally well. The same decrease occurs a few hours later in Figure 16 for the buoy farther to the south.

For wind direction, the values for the 58 minute averages are connected by lines. The X's represent the 8.5 minute averages. The two are not very far apart. The shift in direction is tracked equally well by both the 8.5 and the 58 minute averages.

For these two sets of curves, one is tempted to do a three point running average of the 58 minute averages for speed and direction (or perhaps the vector components) and call the result the synoptic scale wind.

Figure 17 and 18 show only the 58 minute and 8.5 minute speeds and directions and not the gusts. For Figure 17, the 58 minute averages are smoother than the 8.5 minute averages for speed. The direction scale has been enlarged and the 58 minute averages are more smoothly varying than the 8.5 minute averages and are probably more representative of the synoptic scale. Again, a three point running average of the 58 minute averages might be a better representation of the synoptic scale. For Figure 17, the winds vary from 6.5 to 10.5 m/s.

For lighter winds as in Figure 18 the 8.5 minute speeds and directions both fluctuate about the 58 minute averages by large amounts for winds near 5 m/s.

Even the hourly averages are erratic. The air was 2 to 3 degrees Celsius colder than the water during this period, which could have resulted in very unstable conditions for such light winds. For these light winds, a one hour average samples only 18 km of moving air. Perhaps for these light winds, a running 5 hour average might better represent the synoptic scale.

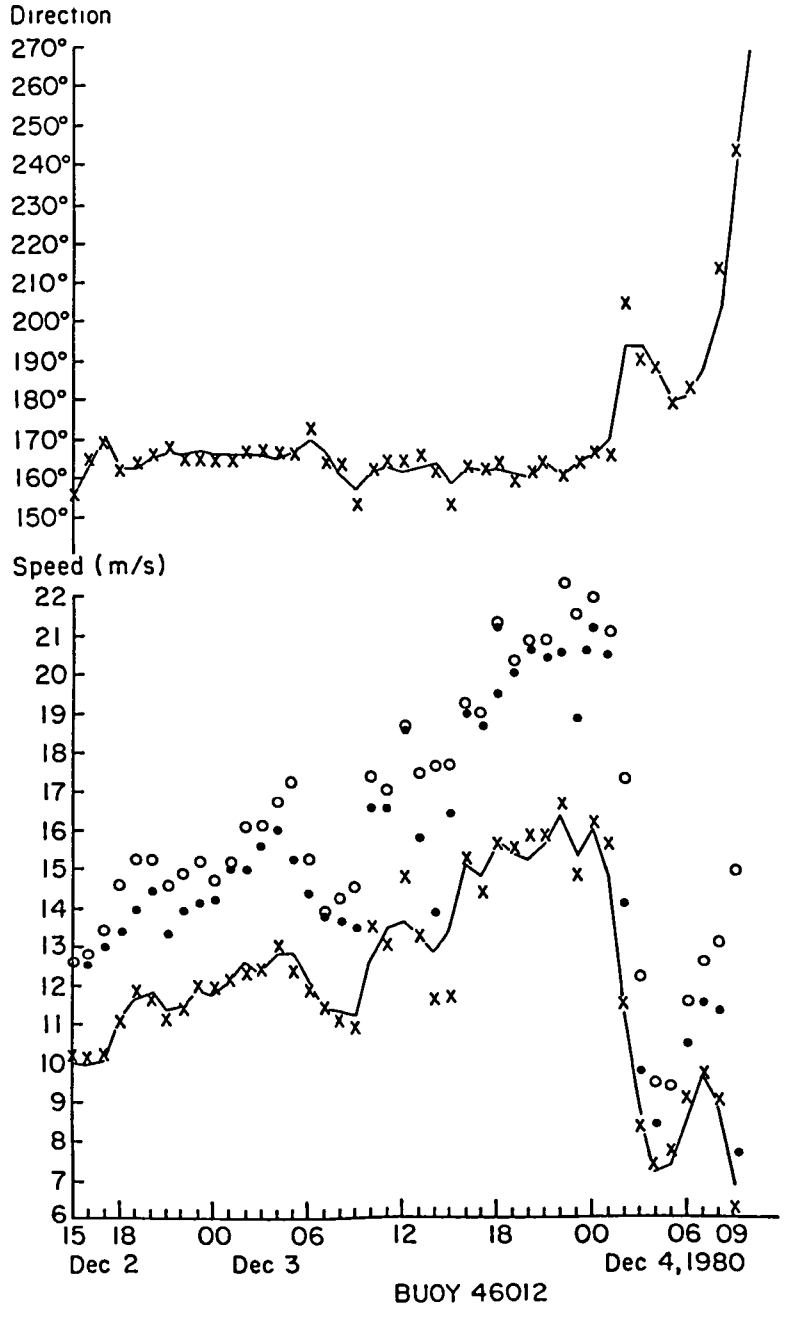

FIGURE 15 Wind speed (ms^{-1}) and direction (degrees) for Station 46012, Dec. 2-4, 1980. (Line, 58 min average; x, 8.5 min average; dot, 8 sec gust during 8.5 min observation; circle, 8 sec gust during 58 min observation).

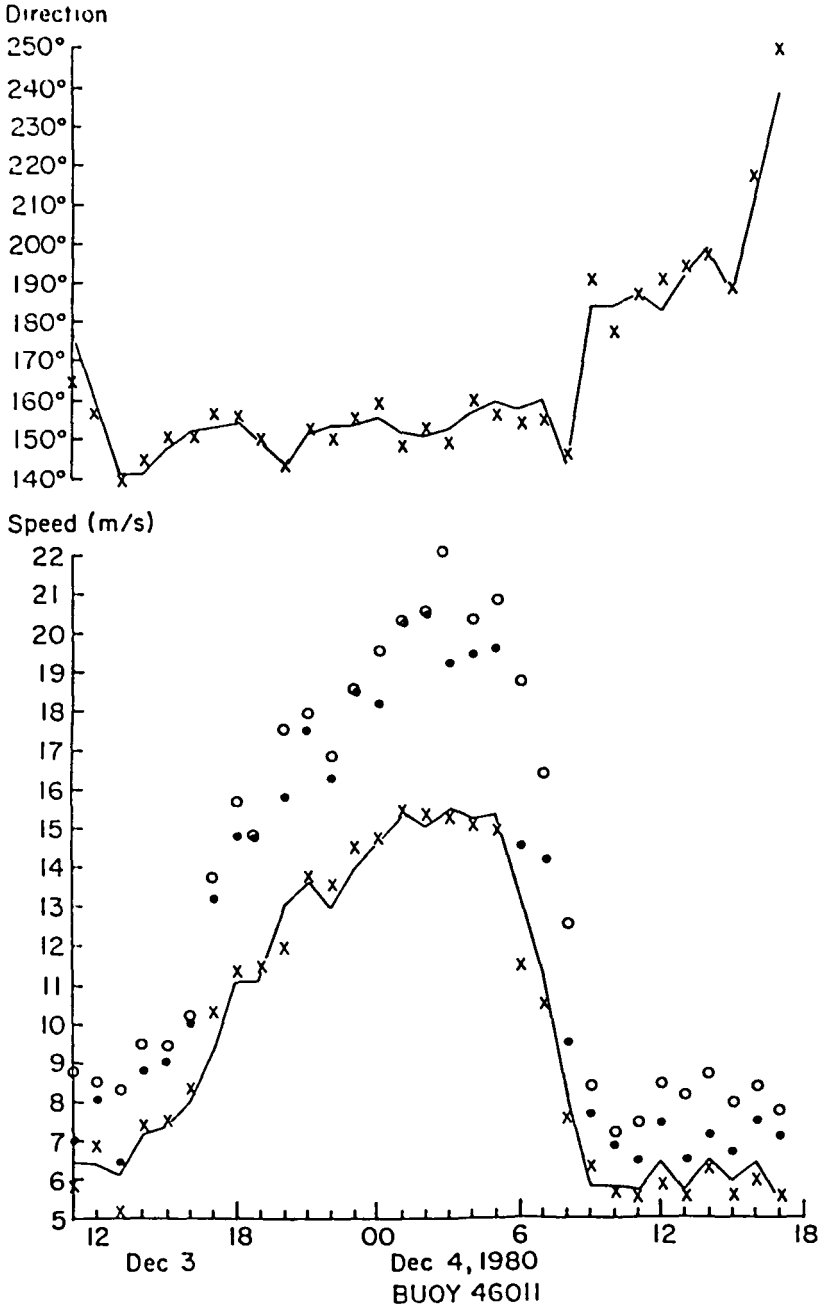

FIGURE 16 Wind speed (ms^{-1}) and direction (degrees) for Station 46011, Dec. 3-4, 1980. (See Fig. 15.)

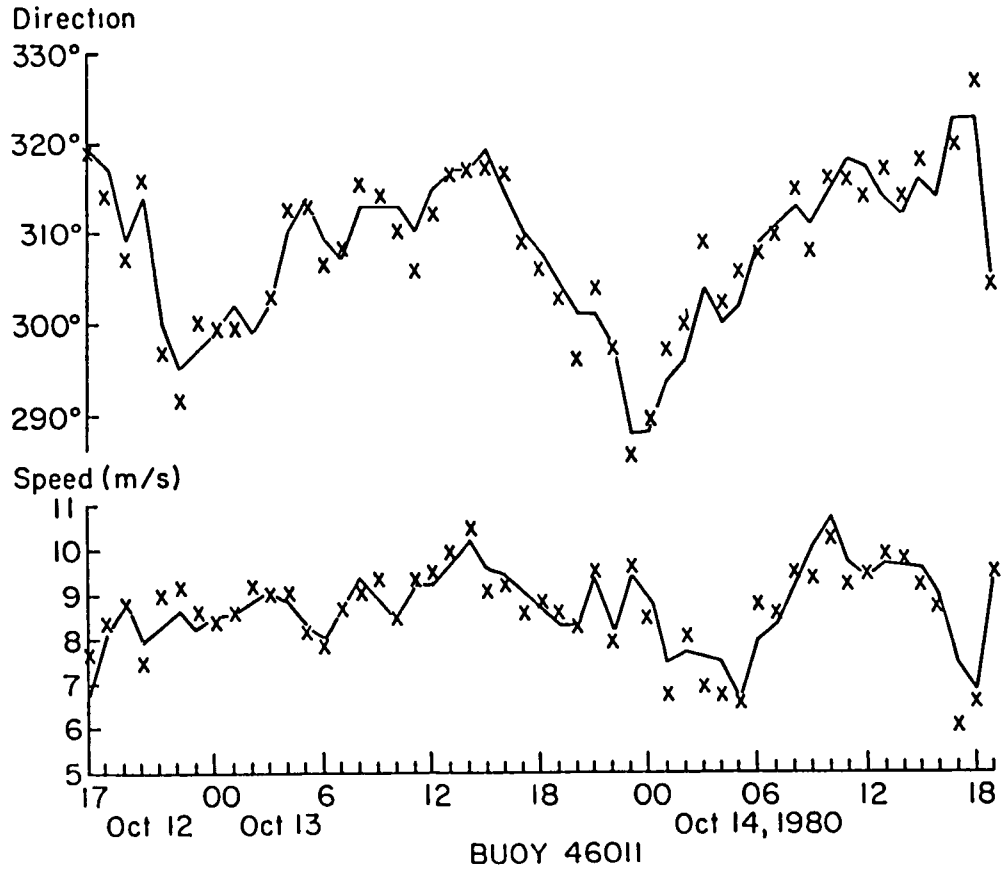

FIGURE 17 Wind speed (m/s) and direction (degrees) for Station 46011, Oct. 12-14, 1980. Jagged line, 58 minute averages. X's 8.5 minute averages.

The mesoscale-microscale spectra that have been obtained and the graphs of the 58 and 8.5 minute averages from the data buoys show that longer time averages of about one hour might be more smoothly varying with time (and hence with distance) and more representative of the synoptic scale wind. It is now possible on the basis of the spectra that have been obtained to determine quantitatively in a statistical sense how much 8.5, or 10 or 2, minute averages will differ from longer averages of 40 minutes, or an hour, or perhaps even longer.

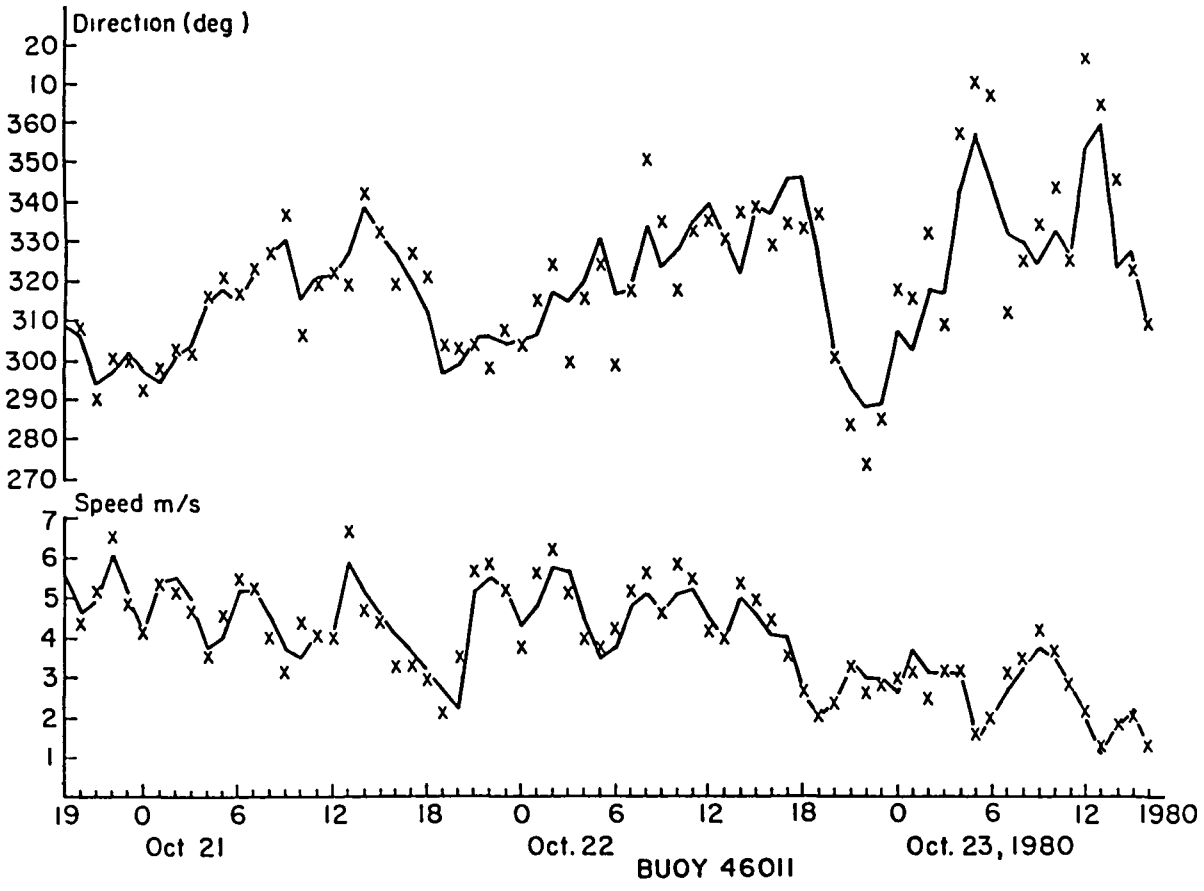

FIGURE 18 Wind speed (m/s) and direction (degrees) for Station 46011, Oct. 21-23, 1980. Jagged line, 58 minute averages. X's 8.5 minute averages.

Consider two time averaged winds, one averaged over T_2 seconds and the other averaged over T_1 seconds, where

$$T_2 > T_1 \tag{63}$$

Then

$$\bar{u}\ (T_2) = \frac{1}{T_2} \int_{-T_2/2}^{T_2/2} u(t)\ dt \tag{64}$$

The fluctuations of u(t) about this average are given by (65).

$$u'(t) = u(t) - \bar{u}(T_2) \tag{65}$$

If these fluctuations are averaged over T_1 seconds, the result is (66).

$$\bar{u}'(T_1) = \frac{1}{T_1} \int_{-T_1/2}^{T_1/2} u(t)dt - \bar{u}(T_2) = \bar{u}(T_1) - \bar{u}(T_2) \tag{66}$$

For many such operations with similar synoptic conditions, it would be anticipated that

$$\text{AVE } (\bar{u}(T_1) - \bar{u}(T_2)) = \text{AVE } \bar{u}'(T_1) = 0 \tag{67}$$

The average value of the square of the difference would not be zero and can be computed as follows, where E is the expectation operator.

$$\text{VAR } (\bar{u}(T_1) - \bar{u}(T_2)) = \text{VAR } \bar{u}'(T_1)$$

$$= E \left\{ \frac{1}{T_1} \int_{-T_1/2}^{T_1/2} u(t)\, dt - \bar{u}(T_2) \right\}^2$$

$$= E \left\{ (\bar{u}(T_1))^2 - 2\, \bar{u}(T_1)\, \bar{u}(T_2) + (\bar{u}(T_2))^2 \right\}$$

$$= E \left\{ (\bar{u}(T_1))^2 - (\bar{u}(T_2))^2 \right\}$$

$$= \int S(n) \left(\frac{\sin \pi n T_1}{\pi n T_1} \right)^2 dn - \int S(n) \left(\frac{\sin \pi n T_2}{\pi n T_2} \right)^2 dn \tag{68}$$

Consequently

$$\bar{u}(T_1) = \bar{u}(T_2) + \zeta\, SD(u') \tag{69}$$

where

$$(SD(u'))^2 = \int S(n) \left[\left(\frac{\sin \pi n T_1}{\pi n T_1} \right)^2 - \left(\frac{\sin \pi n T_2}{\pi n T_2} \right)^2 \right] dn \tag{70}$$

and where ζ is random variable drawn from some probability density function with a zero mean and a unit variance. For many applications, it is more or less satisfactory to assume a unit normal distribution, but the assumption is not really necessary.

Given an analytical form for S(n) the evaluation of the integral in equation (70) can be complicated. If the effect of the filter extends into the microscale portion of either Figure 12 or Figure 14b, the integral could be evaluated by a summation over logarithmically space frequency intervals.

However for many possible values of T_1 and T_2, both filters affect only the mesoscale portion of the spectrum as illustrated by Figure 9. For this situation, only the area under curve 2 and above curve 3 needs to be found. The equivalent square cut-off frequencies are $n_2 = 0.3631(T_2^{-1})$ and $n_1 = 0.3631(T_1^{-1})$. The rectangular area between these two frequencies is then the desired quantity.

For neutral stability, averaging times of two minutes are sufficient to filter out the microscale. For z/L less than -0.5, it is probably necessary to evaluate the integral by a summation. The variability would them be larger than the values tabulated below.

To evaluate equation (70), if only the mesoscale spectrum is involved, note that

$$\frac{df}{f} = \frac{dn}{n} \tag{71}$$

so that

$$(SD(u'))^2 = 0.7614 \int_{n_2}^{n_1} u_*^2 \, \Phi_\varepsilon^{2/3} \frac{dn}{n}$$

$$= 0.7614 \, u_*^2 \, \Phi_\varepsilon^{2/3} \, \ell n \, (n_1/n_2) = 0.7614 \, u_*^2 \, \Phi_\varepsilon^{2/3} \, \ell n \, (T_2/T_1) \tag{72}$$

for wind speeds greater than 10 m/s. Similar equations apply for a wind of 5 m/s.

Suppose that the mesoscale spectrum extends to frequencies corresponding to periods of 2 hours 45 minutes. Then T_2 equal to 60 minutes could give an average wind representative of the synoptic scale so that $\bar{u}(T_2)$ can be renamed $\bar{u}_s$. From (72), it is then possible to compute the variability of a 30 minute average, or of an 8.5 minute data buoy average, or of a 2 minute ship of opportunity average, relative to a 60 minute average.

From Figure 12, a sixty minute average requires shifting the inverse of the dash dot curves $\log_{10} 1.5$ to the left.

The standard deviation of the fluctuations about the synoptic scale average for $\bar{u}_s$ greater than or equal to 10 m/s can be written as equation (73).

$$SD(u') = 0.873\ u_*(\Phi_\varepsilon^{2/3}\ \ell\eta\ (T_2/T_1))^{1/2} \qquad (73)$$

Also $(\ell\eta(60/2))^{1/2} = 1.844$, $(\ell\eta(60/8.5))^{1/2} = 1.358$, and $(\Phi_\varepsilon^{2/3})^{1/2}$

at z/L = -1 is 1.224, at z/L = -0.5, it is 1.146 and at z/L = 0.5,

it is 1.628.

These values plus the entries in Table 8 make it possible to prepare Table 9 with a correction for $\bar{u}_s$ = 5 m/s. For unstable conditions, especially for 2 minute averages, the values in Table 9 may be an underestimate. From Table 9, the variability of the winds measured either by a ship with an anemometer or a data buoy is very large especially for high winds. A synoptic scale analysis based on wind measurements that differ from the synoptic scale wind by the amounts shown would produce errors in the isobaric gradients of 5 to 10% (and sometimes greater). With some averages too high and others too low, the entire isobaric pattern would be distorted. Even if the wind direction were error free, a pressure gradient of 3 mb (0.3 pascals) per 100 km. that was in error by 10% would produce an error in the central pressure for a low of 1.5 mb over 500 km. The standard deviations for 30 minute averages relative to a 60 minute average are also shown. The standard deviations compared to 2 minute average winds from ships are reduced to 45% of their previous values since $(\ell\eta\ 2)^{1/2}/(\ell\eta\ 30)^{1/2} = 0.451$.

TABLE 9 Standard Deviations (m/s) of the Fluctuations of 30, 8 5 and 2 Minute Averages Relative to a 60 Minute Synoptic Scale Average As a Function of Stability and Wind Speed at 10 Meters

z/L	-1.0			-0 5			0			+0 5		
AVERAGING TIME (MIN)	30	8.5	2	30	8.5	2	30	8 5	2	30	8 5	2
$\bar{u}_s$ (m/s)												
5	-	-	-	-	-	-	0.08	0.16	0.21	-	-	-
10	0 35	0.59	0.78	0 31	0.52	0.69	0.25	0.42	0.56	0.34	0.57	0.75
12.5	0.47	0.79	1.04	0.41	0 70	0.92	0.33	0.55	0.73	0.42	0 71	0 94
15	0.62	1.03	1.36	0.53	0.89	1 18	0.42	0.70	0 92	0.52	0.88	1.16
17.5	0.76	1.27	1.68	0.66	1.11	1.46	0.51	0.86	1.14	0.59	0.99	1.31
20	0 92	1.54	2.04	0.80	1.34	1.76	0.61	1.03	1.36	0 65	1.09	1.44
22.5	1.09	1.84	2 43	0.94	1.58	2.08	0.72	1.21	1.60	0.75	1.26	1.66
25	1.28	2.15	2.84	1.09	1.84	2.42	0.84	1.40	1.85	0.97	1.63	2.15

By a similar analysis, the standard deviation of v' for $\bar{u}_{10} \geq 10$ m/s is given by equation (74).

$$SD(v') = 0.763\ u_*(\Phi_\varepsilon^{2/3}\ \ell n(T_2/T_1))^{1/2} \tag{74}$$

Except for a wind speed of 5 m/s, the entries in Table 9 need only be multiplied by 0.763/0.873 = 0.874 to obtain the tables for $SD(v')$. For 5 m/s, the factor is 1.155.

The variability in wind direction for 2 and 8.5 minute averages relative to the synoptic scale average can be found by computing (75).

$$\chi' = \tan^{-1}\ (SD(v')/\bar{u}_{10}) \tag{75}$$

These values are given in Table 10. The values for a 30 minute average would be roughly half of the values for the 2 minute averages.

TABLE 10 Variability of the Wind Direction (Degrees) for the Fluctuations of 8.5 and 2 Minute Averages Relative to a Synoptic Scale Average of 60 Minutes As a Function of Stability and Wind Speed at 10 Meters.

z/L	-1		-0 5		0		+0.5	
AVERAGING TIME (MIN)	8 5	2	8 5	2	8.5	2	8 5	2
$\bar{u}_s$ (m/s)								
5	-	-	-	-	2 1	2 8	-	-
10	3.0	3 9	2.6	3 5	2 1	2.8	2.9	3.8
12.5	3.2	4.2	2.8	3.7	2 2	2.9	2.8	3.8
15	3.4	4 5	3.0	3 9	2.3	3.1	2 9	3.9
17 5	3 6	4.8	3.2	4.2	2 5	3.2	2.8	3.7
20	3 9	5.1	3.4	4.4	2.6	3.4	2.7	3.6
22.5	4.1	5.4	3.5	4.6	2.7	3 6	2.8	3.7
25	4.3	5.8	3.7	4.8	2.8	3.7	3 3	4.3

Ship reports and data buoys are used to compute the initial value specification over the ocean by means of some boundary layer model and to verify synoptic scale forecasts for various time ranges. For neutral and unstable atmospheric conditions winds near 15 m/s as reported by these ship and buoys can differ from the correct synoptic scale wind by anywhere from ± 0.70 to ± 1.4 m/s as rounded standard deviations. Since these speeds are randomly varying, two standard deviations would not be unusual. Similarly, the wind direction at two standard deviations could differ from the synoptic scale value by 10^{o} at times.

The present data density over the ocean rapidly compounds these random mesoscale perturbations of the measurements into distorted isobaric fields and constant pressure surfaces and incorrect initial value specifications. With only one report in a five degree square, not much can be done except to use the wind as reported. Clusters of reports in the same general area can be weighted and averaged, but areas of such high data density are few and far between.

It also follows that even a perfect 48 hour synoptic scale wind forecast of 22.5 m/s when verified against a transient ship report could differ from what the ship reported by ± 2.40 to ± 4.80 m/s. The transient ship was simply not measuring the quantity forecasted by the synoptic scale model.

Most synoptic scale forecasts have wind errors larger than those indicated by Tables 9 and 10 when verified against ship reports and data buoys so that there is room for improvement, but part of the forecast error was caused initially by an incorrect initial value specification. This remaining part is both unavoidable and unpredictable given the present system for measuring and reporting the winds. The details of the mesoscale, such as the exact value of a two minute average of the wind speed and direction, cannot be predicted with a synoptic scale model; only the statistics can be predicted and understood.

If the averaging time to remove the mesoscale variability really should be longer, say, two hours instead of one hour, the values of $(\ell n\ (T_2/T_1))^{1/2}$ in the preceeding equations would not increase by very much. The values in Table 9 and 10 would increase by small amounts.

The best averaging time to obtain a synoptic scale wind may depend on the location of the ship, or buoy, the time of year, and the current synoptic situation. A data buoy in The Bay of Bengal during the summer monsoon season might require six hourly averages for best results.

When the United States NOAA Data Buoy Program was in its design stages, there were numerous constraints on the amount of data that could be recorded and transmitted. These constraints were imposed by battery drain due to both transmission at HF and available circuitry. The 8.5 minute averages of the wind speed once per hour were dictated by these constraints. More modern electronics and UHF transmissions to and from the geostationary spacecraft have removed these constraints.

It has been recommended (Pierson (1981)) that the NOAA Data Buoys record 5, 10 or 12 minute averages continuously, except for 2 minutes each hour for data transmission. These averages can then be averaged for as long a combined time as desired so as to obtain stable values for the synoptic scale wind. Frontal passages and other sudden changes could then be located in time.

For transient ships, one important step would be to increase the averaging time. A 10 minute averaging time as recommended to the World Meteorological Organization by Dobson (1981) would be a step in the right direction, but an even longer averaging time would be still better. It is also important to refer all measurements to the same elevation above the sea surface by means of Monin Obukov theory because of the large variation of anemometer heights on ships.

It is presently feasable (Grey and Krop (1979) Pg. 72) to double the number of transient ships that make reports and double again the number of reports that these ships make. The total result would be 16,000 to 20,000 reports per day as opposed to the present 4,000 to 5,000. The reports from many close-by ships, say 50 to 100 km apart, now take on a new meaning. Their reports of wind speed and direction should not be expected to agree. The ships are sampling different parts of the mesoscale turbulence field. The vector average of the reports located at their center of gravity should be a better estimate of the synoptic scale wind. If p ship reports, each obtaining 10 minute averages of the wind, were clustered around a grid point for a synoptic scale analysis, the standard deviations of the scatter in the measurements would be about $p^{-1/2}$ times the values for an 8.5 minute average given in Tables 9 and 10. The greater the density of ship repors, the better the synoptic scale analysis will be. A factor of four in report density, even if concentrated on the shipping lanes, is well worth the effort. Six ships near a grid point each obtaining a 10 minute average are not the equivalent of one ship obtaining a 60 minute average. The lower mesoscale frequencies are still present in each 10 minute average. Perhaps selected ships could be equipped to obtain longer averages.

Ways to improve conventional ship reports of weather data were described in Grey and Krop (1979). Automated weather stations on transient ships hold promise and may become inexpensive enough for practical use. The question of a much longer more representative averaging time could then be addressed.

REMOTE SENSING

Even if all of the recommendations of the preceding section were implemented, the data base would still be insufficient to define accurately the synoptic scale meteorological conditions over the oceans. For large oceanic areas in the Northern Hemisphere, which is 60% ocean, and for nearly all of the Southern Hemisphere, which is 80% ocean, there are not enough reports to define the synoptic scale accurately. Inexpensive drifting buoys in the Southern Hemisphere that are located by a spacecraft and that report sea level atmospheric pressure and water temperature can provide part of the needed data.

A single instrument on Seasat called the SASS (Seasat A-Scatterometer) measured the winds at about 173,000 points per day during the time it operated for about 92 days. The accuracy of the measurements of speed and direction and the algorithms used to produce the winds are described by Jones et al. (1982) and Schroeder et al. (1982). Improved versions of this instrument are possible and several design configurations are under investigation.

The scatterometer on Seasat (SASS) measured the winds over the ocean by first measuring the normalized radar backscattering cross section at two different aspect angles (about 90^{o} apart) for nearly the same incidence angle. The backscatter was then related to the wind speed and direction at the location of the areas illuminated by the radar by means of a function that was determined by comparing the backscatter measurements and the winds as measured by ships and data buoys.

These baskscatter measurements trade area for time. There are spatial fluctuations in the wind over the ocean that are the equivalent of the temporal fluctuations of the wind in an anemometer record. For the purposes of this paper, the spatial fluctuations will be treated as one dimensional, which is an over simplification that can someday be removed. It is also necessary to advect these rather long eddies without change in form with the mean synoptic scale wind in order to make any progress at all.

Finally, it must be assumed that the gusts and lulls in the wind for the mesoscale affect the sea surface and cause the backscatter to increase and decrease (with perhaps a small time lag) as the wind speed and direction varies at anemometer height. Evidence that this last assumption is at least partially correct has been given by Jones et al. (1981) in a study of the backscatter from the Synthetic Aperture Radar on Seasat. Other evidence is found from the "cats paws" that form, move and disappear as spotty roughened areas on an otherwise calm sea surface during light winds.

For Seasat, a typical cell (or footprint) was about 15 kilometer by 70 kilometer. For a scatterometer in the design stage, cells 10 km on a side to be pooled to form larger cells 50 km on a side are being considered. A value of 30 km will be used as a compromise distance for Seasat since $(15 \times 70)^{1/2} \approx 32$.

The equivalent time it takes an eddy to be advected by the mean wind over a distance, D, is given by

$$T_e = D/\bar{u} \tag{76}$$

and the equivalent frequency is

$$n_e = \bar{u}/D \tag{77}$$

The appropriate non-dimensional frequency is consequently.

$$f = \frac{n_e z}{\bar{u}} = \frac{z}{D} \tag{78}$$

The variance of a radar determined wind, $\bar{u}_R$, (with no measurement error sources) relative to a "synoptic" scale average of 60 minutes is thus given by equation (79) as long as only the mesoscale is involved. Note that the factor, 0.3631, is missing because the space averaging filter produces a curve similar to the time average filters illustrated in Figure 9 and the constant cancels out. The equation is for $\bar{u}$, $\geq$ 10 m/s.

$$\mathrm{VAR}\ (\bar{u}_R - \bar{u}_s) = \int_{z/3600\bar{u}}^{z/D} 0.7614\ u_*^2\ \Phi_\varepsilon^{2/3}\ \frac{df}{f} \tag{79}$$

The integration yields (80) with D in kilometers

$$SD(\bar{u}_R) = 0.873\ u_*\ (\Phi_\varepsilon^{2/3}\ \ell\eta\ \frac{3.6\ \bar{u}_s}{D})^{1/2} \tag{80}$$

and

$$\bar{u} = \bar{u}_s + \zeta\ SD\ (\bar{u}_R) \tag{81}$$

Similarly the variability of the transverse component, $\bar{v}_R$, is given by

$$SD\ (\bar{v}_R) = 0.763\ u_*\ (\Phi_\varepsilon^{2/3}\ \ell\eta\ \frac{3.6\ \bar{u}_s}{D})^{1/2} \tag{82}$$

The variability in wind direction is given by (83).

$$\chi_R = \tan^{-1}\ (SD(\bar{v}_R)/\bar{u}_s) \tag{83}$$

For a fixed cell size, the stronger the synoptic scale wind, the larger the variability of the radar measurement.

In order to show the effect of cell size and wind speed, the equivalent averaging time and 0.873 times the logarithmic factor in (79) have been evaluated separately. The values are shown in Table 11. For 30 and 50 km cell sizes the equivalent averaging times exceed one hour for some light winds. For high winds and a 10 km cell size, the equivalent averaging times are less than those for a data buoy. Most standard deviations are reduced by more than a factor of two for a 50 km cell size compared to a 10 km cell size. Variances are reduced consequently by a factor of four.

TABLE 11: Equivalent Averaging Time (T_e) and Values of $0.873(\ell n(3.6\ \bar{u}_s/D))^{1/2}$ for Various Synoptic Scale Wind Speeds and Cell Sizes. For Missing Values the Averaging Time is Longer than 60 Minutes.

	CELL SIZE					
	10 KM		30 KM		50 KM	
$\bar{u}_s$ (m/s)	T_e, min	Eqn	T_e, min	Eqn	T_e, min	Eqn
5	33.33	0.507*	-		-	
10	16.67	0.988	50	0.373	-	
12.5	13.33	1.071	40	0.556	-	
15	11.11	1.134	33.33	0.619	55.55	0.242
17.5	9.52	1.184	28.57	0.752	47.61	0.420
20	8.33	1.226	25	0.817	41.67	0.527
22.5	7.41	1.262	22.22	0.870	37.07	0.606
25	6.67	1.294	20	0.915	33.33	0.669

*computed from correct equation.

The standard deviations relative to a 60 minute synoptic scale average for various wind speeds, cell sizes and atmospheric stabilities are shown in Table 12. Except for the last two values for a 10 km cell for each stability, all of these standard deviations are lower than those given in Table 9 for data buoys. All values are below those of a 2 minute transient ship average.

TABLE 12 Standard Deviations of Scatterometer Measurement Winds (m/s) Relative to a Synoptic Scale Average of 60 Minutes for Various Values of z/L and the Synoptic Scale Wind Speed. Dashes Indicate an Area Average that is the Equivalent of a Time Average Longer than One Hour.

z/L	-1			-0.5			0			+0.5		
$(\Phi_\varepsilon^{2/3})^{1/2}$	1.224			1.146			1			1.628		
CELL SIZE	10	30	50	10	30	50	10	30	50	10	30	50
$\bar{U}_s$ (m/s)												
S	X	-	-	X	-	-	0.09	-	-	X	-	-
10	0.48	0.18	-	0.43	0.16	-	0.34	0.13	-	0.46	0.17	-
12.5	0.69	0.36	-	0.61	0.32	-	0.48	0.25	-	0.63	0.32	-
15	0.96	0.57	0 20	0.83	0.45	0.18	0.65	0.38	0.14	0.82	0.48	0.17
17.5	1.23	0.78	0.54	1.07	0.68	0.38	0.83	0.53	0.30	0.96	0.61	0.34
20	1.55	1.03	0.67	1 34	0.89	0.58	1.03	0.69	0.45	1.09	0 73	0.47
22.5	1.90	1.31	0.91	1.63	1.13	0.78	1.25	0.86	0 60	1.30	0.90	0.62
25	2.28	1.61	1.18	1.94	1.38	1.16	1.49	1.05	0.77	1.73	1.22	0.89

The variability of the wind direction need not be tabulated. Simple proportions formed from the values in Table 9, 12 and 10 yield the corresponding angles for different cell sizes, stabilities and wind speeds.

In addition to the mesoscale variability of the wind, a scatterometer makes an error in measuring the radar backscattering cross section of a given area of the ocean surface. The backscattered power is embedded in communication noise with the net result that the measured value of σ^o varies randomly about its true value. This source of sampling variability eventually ends up as an error in the wind speed and direction that was recovered from the backscatter measurements. The error is a function of wind speed, wind direction relative to the pointing direction of a reference beam of the radar, incidence angle and the size of the cell being scanned by the radar. Averaged over about 90^o of direction, so as to provide some sample numbers for a radar design called the SCATT, and for an incidence angle near 47^o, these speed errors can be compared to those determined for the SASS in Monte Carlo experiments in which mesoscale variability was not considered as described by Pierson and Salfi (1982) and as summarized in Table 13. Actually, the full details are more complicated because the speed errors are larger for some wind directions and smaller for others. Moreover, the communication noise error is also a function of the incidence angle and is larger for larger incidence angle. The 50 km SCATT cell can be composited from twenty five 10 km SCATT cells. The corresponding errors in direction due to the scatterometer are also given.

TABLE 13 RMS Speed Errors (m/s) and RMS Direction Errors (Degrees) for the SCATT with 10 km and 50 km Cell Sizes and the SASS with a 30 km Cell Size for an Incidence Angle Near 47° As a Result of the Effects of Communication Noise and Attitude Errors

	SCATT	SASS	SCATT*
CELL SIZE	10	30	50
$\bar{U}_s$ (m/s)			
5	0.30/9°	0.50/8°	0.08/2°
10	0.47/5°	0.40/7°	0.22/1°
15	0.76/5°	0.60/6°	0.45/1°
20	1.13/5°	0.90/5°	0.73/1°
25	1.54/5°	1.31/4°	1.07/1°

*Composite of 25 10 km SCATT cells.

The situation of comparing a radar measurement of the wind made with either a SASS or a SCATT and a meteorological measurement of the wind with an anemometer on a data buoy can now be investigated. During GOASEX, the National data buoys made observations every hour on the hour. Suppose that the synoptic scale wind near a data buoy was 15.1 m/s for the hourly observation preceeding a SEASAT pass and that the observation one hour later had a synoptic scale wind of 15.2 m/s. The speeds reported by the buoy would be, from Table 9, for neutral stability,

$$U_{M1} = 15.1 + (0.70)\ \zeta_1 \tag{84}$$

for the first observation and

$$U_{M2} = 15.2 + (0.70)\ \zeta_2 \tag{85}$$

for the second where ζ_1 and ζ_2 would be (zero mean, unit variance, normally distributed, randomly selected) variables to account for mesoscale variability. Suppose that SEASAT passed 20 minutes after the first observation and that U_{M1} and U_{M2} were linearly interpolated to the time of the pass. The meteorologically observed wind speed would then be given by

$$U_M = 15.133 + \frac{2}{3}(0.70)\zeta_1 + \frac{1}{3}(0.70)\ \zeta_2 \tag{86}$$

The SASS would scan two 15 by 70 km cells (which will be assumed coincident for this example). By the time it went by, the mesoscale details of the winds over the "cells" which might be as much as 25 to 50 km

away from the data buoy could be completely different and uncorrelated with what was measured by the data buoy. The wind speed present in the area where the SASS made its measurement could be described by

$$U_c = 15.113 + (0.38)\ \zeta_3 \tag{87}$$

as given in Table 12 as the effect of mesoscale variability. But the SASS had an actual error of measurement that ought to be computed on the basis of the actual (but unknown) mesoscale wind speed and direction present over the pair of cells where the measurement was made. This error can be based approximately on a 15 m/s wind so that the SASS measurement could be represented by

$$U_R = 15.133 + (0.38)\ \zeta_3 + (0.60)\ \zeta_4 \tag{88}$$

where 0.60 is the effect of communication noise for SEASAT from Table 13, and U_R is the magnitude of the wind from the SASS on SEASAT.

The radar wind speed was then compared to the data buoy wind speed by subtracting one from the other which yielded (89). All sources of real errors such as an incorrect model function and errors in buoy calibration have been neglected except the communication noise error of the SASS measurement.

$$U_R - U_M = (0.38)\ \zeta_3 + (0.60)\zeta_4 - (0.70)\left(\frac{2\zeta_1}{3} + \frac{\zeta_2}{3}\right) \tag{89}$$

For repeated measurements near 15 m/s, p such calculations can be made and then the average value of $U_R - U_M$ determines the bias and the mean square value determines the mean square and root mean square "errors". For this example, the bias is zero since the average values of ζ_1, ζ_2, ζ_3 and ζ_4 are zero. The ζ's are independent.

The worst case variance is given by equation (90) since $(1/3)^2 + (2/3)^2 = 5/9$.

$$E(U_R - U_M)^2 = (0.38)^2 + (0.60)^2 + (0.70)^2\ (\tfrac{5}{9}) \tag{90}$$

The variances equals 0.774 m^2/s^2 so that the RMS error is 0.88 m/s. In terms of variance, nearly half of the variance is accounted for by the effects of mesoscale variability on the measurements (0.42/0.774 = 0.54). With no radar error at all, the root mean square difference would still be 0.64 m/s. It would be soley the result of mesoscale variability.

According to the way that the Goasex data were processed, if SEASAT had passed a data buoy exactly on the hour, the 5/9 in (90) would change to a one. The RMS error would then have been 1.0 m/s since the spacecraft measurements would not have been exactly at the location of the data buoy. SEASAT passage at 30 minutes after the hour would have yielded 1/2 instead of 5/9 and produced the lowest RMS error. (A strange result, but correct if the model is realistic).

Mesoscale variability in this example has dominated the synoptic scale trends. Averaging two wind measurements an hour apart produces a better estimate of the wind to be compared to the SASS than using a value closest to the time of the pass or interpolating to the time of the pass.

Similar calculations based on the values given in the various tables can be made for a radar design with 10 and 50 km cell sizes for comparison with the SASS for a 30 km cell size. The details are different, however. The 10 km cell is effectively an 11 minute average for a 15 m/s wind. If the measurement were at the same time as either buoy report, the radar would, to this level of analysis, measure the wind measured by the buoy including mesoscale variability plus the radar communication noise error. If it was 20 minutes later, much of the mesoscale contribution would be independent. For a 50 km cell, the radar would almost measure the synoptic scale wind (± 0.14 m/s) plus the radar error. The cells for the new radar design would always be centered near the buoy. Averaging the two buoy winds an hour apart always helps for the assumed conditions. The results are given in Table 14.

TABLE 14 RMS Differences (m/s) Between Radar Measured Winds and Meteorological Winds Measured with a Data Buoy (Neutral Stratification) for a 15 m/s Synoptic Scale Wind.

RADAR CELL	10 KM	30 KM	50 KM
BEST	0.76* (0 min.)	0.86 (30 min.)	0.68 (30 min.)
OTHER	1.12 (30 min.)	0.88 (20 min.)	0.70 (20 min.)
WORST	1.13 (20 min.)	1.00 (0 min.)	0.84 (0 min.)

*Compared to buoy at same time, the speed could still differ from the synoptic scale wind by ± 1.00 m/s

For wind direction, the corresponding equations would be

$$\chi_M = \bar{\chi}_s + \frac{2}{3}(2.3)\,\zeta_5 + \frac{1}{3}(2.3)\,\zeta_6 \tag{91}$$

$$\chi_R = \bar{\chi}_s + 1.2\,\zeta_7 + 6\,\zeta_8 \tag{92}$$

as found in part from Table 10 and Table 13. Consequently

$$E\,(\chi_R - \chi_M)^2 = 6.4^o \tag{93}$$

and the radar error in measuring the wind duration, in theory, dominates. Since most data buoy reports are to the nearest 10^{0}, the example is academic. Winds from data buoys should probably be reported routinely to the nearest degree in direction.

These tables illustrate how difficult it is to isolate the actual errors in radar scatterometer measurements of the wind. The mesoscale variability of the anemometer measurement depends on averaging time. The mesoscale variability of the radar measurement depends on cell size. The communication noise error also depends on cell size because the smaller the cell size the briefer the signal integration time and the larger the variability of the integrated signal plus noise.

Two situations are illustrated by Table 15. The first shows an attempt to compare conventional ship reports with near by and non-simultaneous radar 10 km cell measurements. The second shows a comparison of 30 minute data buoy measurements with near-by, but not quite simultaneous, radar 50 km cell measurements. In each example, the actual radar error is shown in parentheses. Mesoscale variability, if not taken into consideration, would give the impression that the errors were very large for the 10 km cells.

TABLE 15 Total RMS Variability (m/s) for Two Conditions The Comparison of (I) Two Minute Ship Reports with 10 km Radar Cells and Corresponding Communication Noise and (II) Thirty Minute Data Buoy Reports with 50 km Radar Cells and Corresponding Communication Noise As a Function of the Synoptic Scale Wind Speed (m/s) and z/L. Numbers in Parentheses are the Communication Noise Standard Deviations.

z/L	- 1.0		- 0.5		0		+ 0.5	
$\bar{u}_s$(m/s)	I	II	I	II	I	II	I	II
10	(0 47, 0 22)		1 03	0 41	0.94	0.38	0 72	0 33	1.00	0.40
15	(0 76, 0.45)		1 83	0 79	1 13	0.72	1.30	0.63	1 61	0.71
20	(1.13, 0 75)		2.80	1.36	2.48	1.24	2.03	1.06	2 13	1 10
25	(1 54, 1 07)		3.95	2 04	3 46	1 92	2.89	1.56	3.16	1 70

Suppose now that the data buoy measurements are averaged over about one hour as running centered time averages so that the wind that is reported is the one for the time of the spacecraft passage. The data buoy measurements would then be, by definition (or by assumption), the synoptic scale wind. The cells scanned by SEASAT would still be far enough from the data buoy so that mesoscale effects over the cells would be decorrelated from the anemometer averages. A radar with a 10 km cell size would still obtain the equivalent of an 11 minute anemometer average

for a 15 m/s wind. The 50 km cell would be nearly the equivalent of a one hour anemometer average. The time and space averages could be made essentially coincident for the new radar design and consecutive 10 minute average for the data buoy. The only remaining sources for differences between the buoy measurements and the radar measurements for 50 km resolution except for high winds would then be the communication noise and attitude errors in Table 13 plus true calibration errors for the anemometer on the data buoy.

There is a tendency to oversimplify the interpretation of data. For remote sensing, in general, the comparison data, such as the meteorologically determined winds, have often been treated as if they were correct. Any difference between the remotely sensed quantity and the comparison data is treated as an error made by the remote sensing system. What actually happens is really very different from this oversimplified interpretation. Most of the variability is the result of the fact that the wind speeds at the places and times that the measurements were made were actually different. These differences when compounded in the calculation of statistical quantities such as RMS values account for a large part of the observed variability. They are not actually errors. They are simply differences.

EXAMPLES FROM THE SASS ON SEASAT

SEASAT produced a tremendous volume of data on the winds over the ocean. Those who are using these data to obtain wind fields for synoptic analyses are finding that the winds in an area around a grid point of the synoptic scale meteorological model that they are using need to be averaged to produce a "super-observation" for the model. An analysis can be made to determine the accuracy of the SASS winds for the grid points of a synoptic scale model under the assumption that the mesoscale effects are dominantly uncorrelated and without the use of any of the preceding theory, except as a check. The communication noise effects surely are uncorrelated, and the combined effect would be very weakly correlated, at most, due to the longer wavelength-longer period mesoscale eddies.

Although a more detailed analysis of the effects of communication noise on the wind speed and direction measurements of the SASS on SEASAT suggests that there may be some departure from normality of the probability distribution of speed and direction errors, these departures are dominantly for light winds. Also, the full details of the space-time structure of mesoscale turbulence need a more adequate description.

It is nevertheless worthwhile to see how well the results of the previous section compare to results obtained by SEASAT during the GOASEX experiment. For a wind near 15 m/s, for cells scanned by SEASAT, equations (88) and (92) can be reduced to equations (94) and (95) because mesoscale and communication noise effects cannot be separated in the SASS data.

$$u_R = u_s + 0.71\ \zeta_9 \tag{94}$$

$$\chi_R = \chi_s + 6.12\ \zeta_{10} \tag{95}$$

Figure 19 shows one of the earlier results of the GOASEX program as described in Barrick, et al. (1980) and by Pierson (1981b). The algorithms have been improved since this study, but the model function in use at that time did fairly well for wind speeds from 10 to 15 m/s. There are 16 SASS winds clustered around the oceanographic ship, the "Oceanographer" as extracted as a small sample from an orbit segment obtained over the North Pacific. The SASS winds extend from about 47.6° N to 49.6° N and from 221° E to 223° E. Typically, an area this size has to be represented by a single wind speed and direction for a computer model of the atmosphere at the synoptic scale.

The area involved in Fig. 19 is about 32,600 square kilometers so that each measurement represents about 2000 square kilometers, or a square about 45 km on a side. On the average the radar measurement points are consequently also about 45 km apart, which corresponds to a 50 minute travel time for the movement of eddies from one point to the next for a 15 m/s wind.

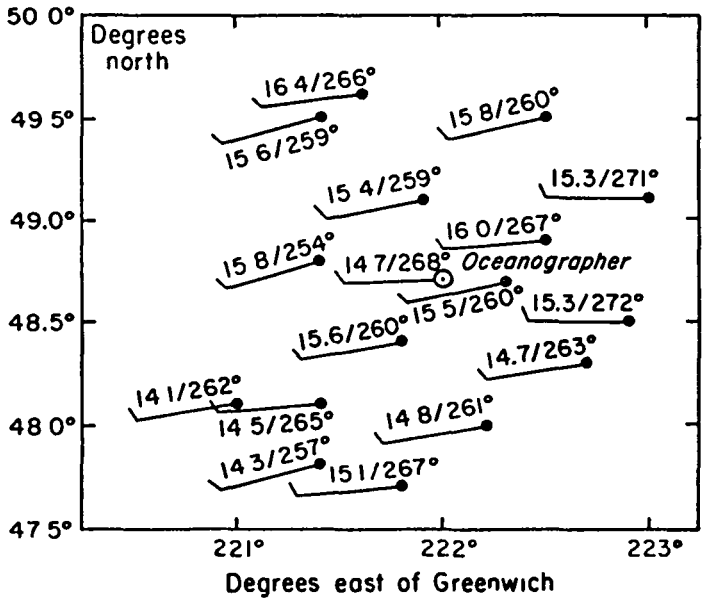

FIGURE 19- SASS high-resolution wind field in the vicinity of the Oceanographer in the North Pacific for orbit 1140. (From Pierson (1981b), for both Figs. 19 and 20, the winds have been referred to 19.5 meters, and the variability about a given winds speed and direction has been assumed the same at this hight).

The average value of the wind speed for p SASS cells is given by (96)

$$\bar{u}_R = \frac{1}{p} \sum_i (u_s + 0.71\ \zeta_{9_1})$$

$$= u_s + (\frac{1}{p} \sum_i \zeta_{9_1})\ (0.71)$$

$$= u_s + \zeta_{11}\ (0.71/p^{1/2}) \qquad (96)$$

and the average value of the direction is given by (97)

$$\chi_R = \chi_s + \zeta_{12}\ (6.12/p^{1/2}) \qquad (97)$$

(where ζ_{11} and ζ_{12} are zero mean unit variance normally distributed random variables) by the same analysis. These equations follow because the average value of p independent samples from a normal distribution has a normal distribution with the same mean and a standard deviation reduced by $p^{-1/2}$. The theory developed so far is thus capable of predicting the reduction in the variability of the wind when scatterometer cells are combined for a larger scale synoptic analysis.

The actual data in Figure 19 can be used to calculate the corresponding values directly without recourse to the turbulence theory. Then the two different results can be compared. The 16 wind speeds in this example range from 14.1 m/s to 16.4 m/s. The average value is 15.23 m/s. The unbiassed estimate of the variance is 0.4092 $(m/s)^2$, and the standard deviation is 0.64 m/s.

A sample of size 16 is a rather small sample. Also the mean, that is the synoptic scale wind, is not actually known. The quantity,

$$\frac{(\bar{u}_R - \bar{u}_s)}{(0.4092)/16)^{1/2}}$$

has a student t distribution. The 90% confidence interval on the estimate of the synoptic scale wind speed is given by (98).

$$\bar{u}_s = \bar{u}_R \pm 0.28 = 15.23 \pm 0.28 \tag{98}$$

The 90% range for a normal distribution with a standard deviation given by 0.71/4 is ± 1.64(0.21), or 0.35, which would be predicted by the model.

The variance (σ_u^2) of a normally distributed random variable is not well estimated by a sample of 16 value. The quantity,

$$15(0.4092)/\sigma_u^2,$$

has a Chi Square distribution with 15 degrees of freedom. The 90% confidence interval on the variance is given by (99),

$$P(0.246 < \sigma_u^2 < 0.845) = 0.90 \tag{99}$$

and the confidence interval of the standard deviation is thus (100).

$$P(0.495 < \sigma_u < 0.919) = 0.90 \tag{100}$$

The standard deviation of 0.64 m/s estimated from the 16 SASS winds compares favorably to the value of 0.71 m/s from the mesoscale-microscale turbulence theory, given the considerable range of the confidence interval.

Also, 69% of the wind speeds in the sample are within plus or minus one standard deviation of the estimate of the mean. The sample is not atypical of a small sample from a normal distribution.

For the wind directions, the 16 SASS values range from 254^{o} to 272^{o}. The average value is 262.69^{o} and the unbiassed estimate of the variance is 24.63 $(\text{degrees})^2$. The 90% confidence interval on the synoptic scale wind direction is given by

$$\bar{\chi}_s = 262.69^{o} \pm 2.17^{o} \tag{101}$$

and the standard deviation has a 90% confidence interval given by

$$P(3.84^{o} < \sigma_{\chi} < 7.13^{o}) = 90^{o} \tag{102}$$

The data from this sample of 16 SASS winds again supports the direction variability of 6.12^{o} predicted by the model.

The "Oceanographer" obtained a 30 minute average of the wind. The model predicts standard deviations of 0.42 m/s and 2.42^{o} for an anemometer averaged wind of 30 minutes. There is a 90% chance that the synoptic scale wind speed is within 14.7 ± 1.65 (0.42) and that the direction is $268^{o} \pm 1.65\ (2.42)^{o}$. The 90% region for the 16 SASS values is from 14.95 to 15.51 m/s; for the "Oceanographer" it is 14.01 to 15.39. The two intervals overlap from 14.95 m/s to 15.39 m/s and include the average of the SASS wind speeds of 15.23 m/s. For direction, the 90% range for the SASS is 260.8^{o} to 265.2^{o}, and for Oceanographer it is 264^{o} to 272^{o}. The common interval is 264^{o} to 265.2^{o}, within one degree of the SASS average direction.

It is difficult to claim that either the SASS average or the "Oceanographer" is the correct value and that there are errors in speed of 0.53 m/s and in direction of 5^{o}. The only real known errors were the backscatter measurement errors (communication noise) of the SASS and they were reduced by a factor of four when the sixteen winds were averaged. The "Oceanographer" may well have obtained a very accurate 30 minute average. The SASS 16 cell average is probably extremly close to the synoptic scale wind. The two values are different, but neither is necessarily incorrect.

Figure 20 shows a second example in which a data buoy 8.5 minute average is compared to 12 SASS measurements clustered around it. The analysis of the data in this figure is summarized in Table 16. The range of wind speeds for the data buoy compares favorably to the range of speeds for the super observation, and the super observation point estimate for the speed of 9.43 m/s is within the range of speeds for the data buoy. The wind directions do not quite agree. The actual direction variability for the SASS observations may be greater than given in Table 13 for this actual wind direction. The upper limit on the confidence interval for wind direction variability as estimated from the 12 SASS values would provide a wide enough interval to explain the data buoy wind direction.

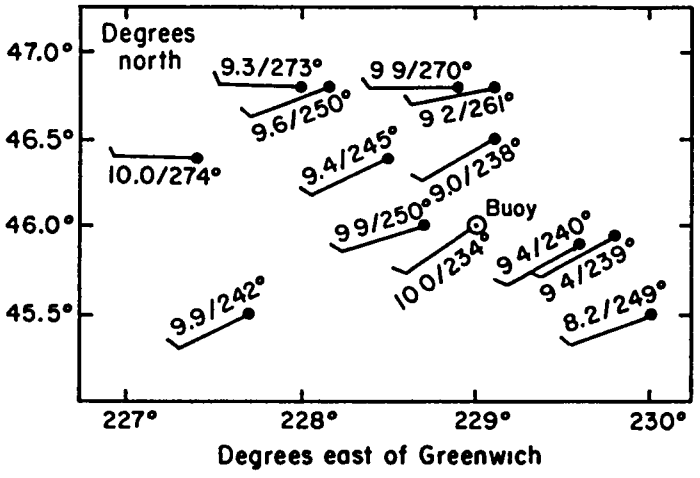

FIGURE 20-SASS high-resolution wind field in the vicinity of data buoy 46005 in the North Pacific for orbit 1140 (From Pierson (1981b)).

TABLE 16 Summary of Analysis for Figure 20

DATA BUOY, $\bar{u}_{8.5} = 10$ m/s, $SD\bar{u} = 0.42$ m/s

$\bar{\chi}_{8.5} = 234^{o}$, $SD\bar{\chi} = 2.1^{o}$

90 % probability range, 9.31 to 10.69 m/s, 230.5^{o} to 237.5^{o}

12 SASS CELLS 9.2 to 10 m/s, 238^{o} to 274^{o}

$\bar{u}_R = 9.43$ $SD\bar{u} = \pm 0.50$ m/s

$\bar{\chi}_R = 252.6^{o}$ $SD\bar{\chi} = 13.49^{o}$

Neutral Theory (10 m/s) $SD\bar{u} = 0.42$ m/s $SD\bar{\chi} = 7.03^{o}$

90% probability range, 8.61 to 10.26 m/s, 230.3^{o} to 278.5^{o}

Super Observation (student t 12 degrees of freedom and Chi Square 11 degrees of freedom)

$\bar{u}_s = 9.13 \pm 0.26$ m/s, 90 % range, 9.17 to 9.69 m/s

$\bar{\chi}_s = 252.6^{o} \pm 6.9^{o}$, 90% range, 245.7^{o} to 259.5^{o}

P (0.37 m/s σ_u <0.78 m/s) = 0.90

P ($10.1^{o} < \sigma_{\chi} < 20.8^{o}$) = 0.90

Another important feature of the individual SASS winds in Figures 19 and 20 is that any apparent pattern is a fiction of random effects of the communication noise. The winds do not represent any real mesoscale features. The communication noise plus mesoscale variability errors, although random and dominantly uncorrelated, have the unfortunate propensity to form quasi-organized patterns over the field under analysis.

It may be advisable to smooth vector component fields that result from the gridded super-obs before forming a vector wind stress field and any derivative fields. Since the values of SD(u) and SD(χ) are derivable theoretically, the difference between any smoothed field and a super ob field should illustrate certain statistical properties associated with randomness and the theory of runs.

The inherent scatter of present ship reports and data buoy reports as shown in Tables 9 and 10 plus their sparse distribution over the oceans must introduce errors in present synoptic scale analyses even if the most modern concepts are used as described by McPherson, et al. (1979), Bergman (1979) and Gill, et al. (1979). The error fields for conventional data are one of the major reasons for poor numerical weather predictions in the three to four day time frame because their effects dominate the forecast. The errors of a super ob wind field will be much much smaller than the errors of the wind fields obtained by the analysis of conventional ship of opportunity winds. The 173,000 winds per day such as those in Figures 19 and 20, when pooled in groups of 16, provide 10,800 uniformly spaced observations for vastly improved synoptic scale analyses with errors (in the sense of departures from the synoptic scale) comparable to those just calculated.

SOME SCATTEROMETER DESIGN CONSIDERATIONS

The SASS on SEASAT achieved the level of accuracy documented in the papers cited previously and in the analyses given in this paper. Improved scatterometer designs based on recent technological advances and on the study of the data from SASS are already under consideration. One of these possible designs is the SCATT as studied for example, by Pierson and Salfi (1982) for which various features have been described above.

A summary for neutral stability of the contributions from mesoscale variability and communication noise for three cell sizes and four wind speeds is given in Table 17. For some wind directions, the communications noise effect on wind direction is much greater than tabulated.

Any mesoscale information at a 10 km resolution of the kind analysed in this model is completely masked by the added communication noise variability. By means of equations (88) and (92), Monte Carlo simulations of typical wind fields could be generated, first by generating a mesoscale field and then by adding the effects of communication noise. By inspection of Table 17, the mesoscale features described by this model would be difficult, if not impossible, to recover once the communication noise effects are added for all scales of resolution and especially for a 10 km resolution.

TABLE 17 Scatterometer Design Standard Deviations in Wind Speed and Wind Direction for a Neutral Atmosphere and 10, 30 and 50 km Cell Sizes (Speed in M/s, Direction in Degrees).

Wind speed, m/s	CELL SIZE	10 KM (SCATT)			30 KM (SASS)			50 KM (SCATT)		
		Meso-scale	Comm. Noise	Total	Meso-scale	Comm. Noise	Total	Meso-scale	Comm. Noise	Total
10	SPEED	0.34	0.47	0 58	0.13	0 40	0.42	0	0.22	0.22
	DIRECTION	1.7°	5°	5.3°	0.65°	7°	7 03°	0	1.0°	1 0°
15	SPEED	0.65	0.76	1.00	0.38	0.60	0 71	0.14	0 45	0.47
	DIRECTION	2.1°	5°	5.4°	1.2°	6°	6.11°	0.46°	1.0°	1.1°
20	SPEED	1.03	1 13	1 53	0.69	0 90	1.13	0.45	0.73	0 86
	DIRECTION	2.6°	5°	5.6°	1.7°	5°	5.3°	1.1°	1.0°	1.5°
25	SPEED	1.49	1 54	2.14	1.05	1.31	1 68	0.77	1.07	1.32
	DIRECTION	3 0°	5°	5.8°	2.1°	4°	4 5°	1.5°	1.0°	1.8°

Much the some thing also happens for the SASS at its coarser resolution. The SASS direction errors from communication noise mask the mesoscale contribution. The super-observation overcomes even this effect for realistic synoptic scales.

Strangely enough, the 50 km resolution still has communication noise and mesoscale effects that are not too different for high winds. They are not quite what would be expected by dividing the 10 km values by five since twenty-five ten by ten kilometer cells are the equivalent of one fifty by fifty kilometer cell.

A factor of three in linear cell size with the design improvement of the SCATT still gives standard deviations almost as small as those of the SASS. Moreover, the ten kilometer cells more uniformly cover the area to be sampled. The higher resolution was gained by compromising the integration time for each measurement and decreasing the area sampled. The new design improved the signal to noise ratio so that not too much was lost.

The effects of mesoscale turbulence permeate the problem as a nuisance factor in efforts to obtain a synoptic scale wind. Averaging anemometer winds for much longer times than those presently used, or planned, will aid in synoptic analyses. Averaging scatterometer winds will provide more representative synoptic scale winds for the grid points of a model.

The resolution to be used for a new scatterometer system is a part of its design problem. The penalty for high resolution is three fold. Firstly, it decreases the signal to noise ratio of the measured backscatter signals with a resulting increase in the errors of the wind speeds and directions calculated from the measurements. Secondly, the smaller cell size has an average wind over it that differs because of these mesoscale effects from the synoptic scale wind. Table 17 shows that of these two effects the increased communication noise error dominates the effects of mesoscale variability. Thirdly, the data rates and data processing requirements vary inversely as the square of the desired resolution.

The ten kilometer resolution would be of value for wind fields over the ocean such as those in hurricanes and tropical storms when strong gradients over short distances are found. Other types of mesoscale features can, of course, have gradients in speed and variations in direction that would stand out above the communication noise effects present for a high resolution. However, most of the time, over most of the ocean, the effects described in this paper will dominate.

A ten kilometer resolution is a bit much, even for coastal studies. For relatively small sample sizes, increasing the sample size by a factor of two reduces the sampling variability effect by dramatic amounts. A 15 or 20 km resolution with either the 15 by 15 km cells pooled in groups of 16 to provide 60 km by 60 km resolution most of the time or the 20 by 20 km cells pooled in groups of 9 to provide 60 by 60 km resolution most of the time might recover enough signal to noise to reduce the communication noise by enough to reveal mesoscale features with these scales. For scatterometers on spacecraft of the future, which will surely be built, further design studies before a final decision is made are definitely needed.

NEEDED MESOSCALE AND MICROSCALE RESEARCH

It is important to understand more about the particular kind of mesoscale activity studied in this paper. Eddies with one horizontal space dimension tied to time by Taylor's hypothesis may be realistic enough as a start in attempting to understand the mesoscale. The actual turbulence structure is more complicated requiring the definition of $u = \bar{u}(z) + u'(x, y, z, t)$, $v = \bar{v}(z) + v'(x, y, z, t)$ and $u_*(x, y, t)$ as a minimum in the planetary boundary layer. The wave number-frequency relationship is undoubtedly not that of Taylor's hypothesis. Most studies in the microscale do not cover a sufficient range of frequencies and heights above the sea surface to provide the kind of data needed.

There may be long cylindrical roll vorticies oriented roughly parallel to the wind under some circumstances as described in detail in a review by Brown (1980). The presence, or absence, of any quasi-organized motions within an area scanned by the radar cells is difficult to demonstrate. If present, they are not so dominant a feature as to be readily obvious in anemometer data as illustrated in Pierson, et al. (1980). Most theories of turbulence are adequate for the microscale, but better theories are needed for the mesoscale range of periods. They should be related to the thickness of the Ekman boundary layer and to Monin-Obukov scaling. The scaling used in this study (equation 11) has not always been associated with the longer period gusts in the planetary boundary layer. Davenport (1961) used a much longer length scale instead of the height of the anemometer in a similar scaling.

It is necessary to understand the scatter in data such as the data in the work of Smith (1980) and many other investigators. As another example, Large and Pond (1981) write that "The dependence of the neutral drag coefficient at 10 meters on wind speed was approximated by equation (10). Using the formulation, the bulk aerodynamic method gave good measures of the momentum flux averaged over a day or two and good hourly averages when the wind was steady. Over periods nearing a day, the bulk and dissipation estimates could consistently differ by as much as 30% . Discrepancies were associated with varying winds, with the dissipation estimates being smaller on the rising wind, and larger on the falling wind, of after a change in wind direction. The surface roughness, and hence drag coefficient, may depend on sea surface parameters that are a product of both past and present winds". The suspicion exists that the stress of the wind on the sea surface is not simply a function of the average wind.

The work of Soulsby and Dyer (1981), although applied to the behavior of time varying ocean tidal currents above the bottom, can equally well be applied to the wind profile. The profile is no longer characterized as solely a function of the friction velocity for neutral stability. It is also a function of the time rate of change of the friction velocity.

CONCLUSIONS

There is a misfit between both the conventional ways that winds are measured at sea and the remote sensing methods that have recently been proven and the major use for the wind data, which is to obtain synoptic scale analyses of the field of motion and the field of mass over the ocean for numerical weather predictions. Wind measurements by transient ships and data buoys are not averaged for a long enough time to filter out the high frequencies relative to the synoptic scale in the wind fluctuations that belong to the mesoscale. The use of a high resolution scatterometer introduces two sources of variability in the wind measurements; one is the mesoscale variability of the cells being sampled and the other is the error introduced by increased communication noise as a result of decreased sampling time.

The statements are based on data from meteorological towers located in the North Atlantic, Lake Ontario and the North Sea and from the SASS on SEASAT. The data show that there is a portion of the spectrum of the u and v components of the wind that extends from frequencies corresponding to an hour, or so, to frequencies corresponding to several minutes and over a corresponding range of wave numbers and wave lengths. Frequencies lower than these correspond to the synoptic scale and frequencies higher than these to the microscale. The spectrum of the wind (as n S(n) versus $\log_{10}$ n) is often higher on both sides of this frequency band. This band of frequencies is called the mesoscale valley in the spectrum. The spectrum of the mesoscale valley and of the microscale is shown to depend on the speed of the synoptic scale wind and on atmospheric stability.

The results presented in this paper have immediate applications toward improving the observations of winds at sea. Stated simply, even the crude model that has been used shows that the mesoscale variability of the winds ought to be filtered out of transient ship, weather ship and data buoy reports by means of longer averaging times. Usually, the measurements of the wind by a scatterometer ought to be averaged to form super observations before being used in a synoptic scale analysis.

The kind of mesoscale variability studied in this paper is ubiquitous and irrelevent for the synoptic scale. Even if the full details of this scale of motion could be observed instantaneously over the entire ocean, these details would undoubtedly change completely in a short time. They are unpredictable at the present state of the art and will remain unpredictable. They are a part of the turbulence problem and not a part of the synoptic problem. Only their statistical properties need to be predicted and used in the interpretation of wind reports at sea.

The optimum averaging time for the winds is certainly not the present value of two minutes. It is probably closer to one hour than to ten minutes, and it is also dependent on the synoptic scale conditions at the time and place of the measurement. An averaging time of ten minutes would be an improvement, but times of twenty and thirty minutes, or longer, would be even better. Quandrupling the actual number of ship reports could provide an improvement in meteorological forecasts. The average of the winds reported by a cluster of close-by ships provides a more accurate synoptic scale value.

For data buoys, the decision as to the best averaging time can be made after the fact by having them report, say, ten minute averages obtained continuously. The present design and communication system for these buoys makes it possible for them to report, say, 12 numbers each hour for such measurements plus other data on gusts and turbulence values.

For scatterometers on spacecraft of the future, high resolution will be of value for areas of high wind speeds and large wind gradients. Most of the time, the scatterometer measurements should be pooled to produce 50 or 60 km cells, and even these winds need to be further averaged to produce very accurate synoptic scale winds for the grid points of a numerical model. Further design studies for future scatterometers are needed because the cost of too high a resolution is increased communication noise effects which often obscure the mesoscale information being sought.

ACKNOWLEDGEMENTS

The first version of this paper was an attempt to treat the same subject by R. Salfi, R. S. Dischel, G. Baeslack and me that was not quite on the right track and was described in reduced form in the GOASEX II volume. A second version was prepared for the NASA Langley Research Center under contract No. NAS-1-15669. The third and last versions were prepared for NASA under contract NAGW-266.

The second version went through a second iteration after review by L. C. Schroeder, E. M. Bracalente and W. L. Grantham of NASA LaRC and by Professor C. M. Tchen of City College. The comments and suggestions of the reviewers of the second and third versions have been carefully considered for the final version. My thanks to these reviewers.

The spectra provided by Dr. Mark Donelan of the Canadian Centre for Inland Waters, the time series of one minute averages from Dr. Klaus Hasselmann and the National Data Buoy data provided by Mr. John Wilkerson are acknowledged with appreciation. Dr. Donelan was most helpful during the preparation of this last version by providing many references and by his explanations of numerous obscure aspects of microscale turbulence theory. Professor K. L. Davidson and Mr. R. J. Strickler of the U.S. Naval Postgraduate School have obtained results that further support Figures 6 and 7 to be published shortly. Mr. R. E. Salfi was most helpful in evaluating various functions for the preparation of some of the figures. Dr. Victor Delnore proof read the final manuscript and suggested many important corrections.

REFERENCES

Adamo, L. C., G. W. Withee and J. M. Syck (1971): National Data Buoy Project: An estimate of environmental stationary errors. Lockheed Report No. 24430 Lockheed Missiles and Space Company, San Diego, California.

Augstein, E., H. Hoeber and L. Krugermeyer (1974): Fehler bei temperatur-feuchte-und windmessungen auf schiffen in tropischen breiten "Meteor" Forsche-Ergebnisse Reihe B No. 9 Seite 1-10 Berlin-Stuttgart.

Baer, L., H. Chin, R. Erickson, D. P. Hanim, R. W. Severance, Jr. and J. C. Vermeulen (1972): Summary of natural variability study. Lockheed Report No. 25404 , Lockheed Missiles and Space Division, San Diego, CA.

Barrick, D. E., J. C. Wilkerson, P. Woiceshyn, G. H. Born and D. Lame (1980): Seasat Gulf of Alaska Workshop II Report, NASA Jet Propulsion Laboratory Report 622-107 Pasadena, Calif. 91103.

Bergman, K. H. (1979): Multivariate analysis of temperature and winds using optimum interpolation. Mon. Wea. Rev. Vol. 107 No, 11 Nov. pp. 1423-1444.

Blackman, R. B. and J. W. Tukey (1958): The measurement of power spectra from the point of view of communications engineering Bell System Tech. Jour. Jan. and March Vol. 37 (also in book from, Dover, New York).

Brown, R. A. (1980): Longitudinal instabilities and secondary flows in the planetary boundary layer: A review. Reviews of Geophysics and Space Physics Vol. 18 No. 3 pp. 683-697.

Brown, R. A., V. J. Cardone, T. Guymer, J. Hawkins, J. E. Overland, W. J. Pierson, S. Peterherych, J. C. Wilkerson, P. M. Worceschyn and M. Wurtele (1982): Surface wind analyses for SEASAT. J. Geophys. Res. Vol. 87 C5 pp. 3355-3364.

Brown, H. E. and D. A. Olson (1978): Performance of NMC in forecasting a record breaking winter storm, 6-7 February 1978. Bull. Amer. Meteorol. Soc. Vol. 59 No. 5 562-575.

Businger, J., R. H. Stewart, T. Guymer, D. B. Lame and C. H. Born (1980: SEASAT JASIN Workshop Report Rep. 80-62 Jet Propul. Lab. Pasadena Calif.

Cane, M. A. and V. J. Cardone (1981): The potential impact of scatter-ometry on oceanography in Gower J. F. R. Oceanography from Space Plenum Press.

Clancy, R. M., J. D. Thompson, H. E. Hurlburt and J. D. Lee (1979): A model of mesoscale air-sea interaction in a sea breeze-coastal upwelling regime. Mon. Wea. Rev. Vol. 107 No. 11 Nov. pp. 1476-1505.

Davenport, A. G. (1961): The spectrum of horizontal gustiness near the ground in high winds. Q J R M S Nov. 1961 Vol. 87, pp. 194-211.

Dobson, F. W. (1981): Review of reference height for and averaging time of surface wind measurements at sea. Report No. 3 Marine Meteorology and Related Activities W M O Geneva Switzerland (WMO Tech. report in preparation 1982).

Fujita, T. T. (1981): Tornadoes and downbursts in the context of generalized planetary scales. J. Atmos. Sci., Vol. 38 No. 8 pp. 1511-1534.

Gibson, M. M. (1963): Spectra of turbulence in a round jet. J. Fluid Mech. Vol. 15 Part 2 pp. 161-173.

Gill, M., M. Halem, and R. Atlas (1979): Time continuous assimilation of remote-sounding data and its effects on weather forecasting. Mon. Wea. Rev. Vol. 107, No. 2, pp. 140.

Grey, J. and E. Krop (1979): Potential Applications of Aerospace Technology in the Marine Transport Industry. AIAA Aerospace Assessment Series, Vol. 3, AIAA 1290 Ave. of the Americas N.Y., N.Y. 10019, pp. 146

Gyakum, J. R. (1980): On the evolution of the Q E II storm. Preprints Eighth Weather Forecasting and Analysis Conference AMS Boston 23-28.

Jones, W. L., V. E. Delnore and E. M. Bracalente (1981): The study of mesoscale ocean winds in Beal, R., P. S. DeLeonibus and I. Katz. Eds Spaceborne Synthetic Aperture Radar for Oceanography. Johns Hopkins University Press. The Johns Hopkins Oceanographic Studies, No. 7.

Jones, W., L. Schroeder, D. Boggs, E. Bracalente, R. Brown, G. Dome, W. Pierson and F. Wentz (1982): The SEASAT-A satellite scatterometer: The geophysical evaluation of remotely sensed wind vector. J. Geophys. Res. Vol. 87, C5, 3297-3317.

Kaimal, J. C., J. C. Wyngaard, Y. Izumi and O. R. Cote (1972): Spectral characteristics of surface-layer turbulence. Quart. J., Roy. Meteorol. Soc. Vol. 98 pp. 563-589.

Kidwell, K. B. and W. R. Seguin (1978): Comparison of mast and boom wind speed and direction measurements on U. S. GATE ships. NOAA TECH. REP. EDS. 28.

Large, W. G. (1979): The turbulence fluxes of momentum and sensible heat over the open ocean during moderate to strong winds. PH. D. Thesis, University of British Columbia.

Large, W. G. and S. Pond (1981): Open ocean momentum flux measurements in moderate to strong winds. J. Phys. Ocean. Vol. 11, pp. 324-336

Laurmann, J. A. (1978): Comments on weather and climate forecasting as problems in hydrodynamics. Month. Weather Rev. Vol. 106 No. 12 pp 1742-1747.

Leavitt, E. (1975): Spectral characteristics of surface layer turbulence over the tropical ocean, J. Phys, Ocean Vol. 5 No. 1 pp. 157-163.

McBean, G. A. (1971): The variation of the statistics of wind, temperature and humidity fluctuations with stability. Boundary Layer Meteorology 1 pp. 438-457.

McPherson, R. D., K. H. Bergman, R. E. Kytler, G. E. Rasch and D. S. Gortlon. The NMC operational global data assimilation system. Mon. Wea. Rev., Vol, 107, NO. 11 Nov. pp. 1445-1461.

Miyake, M., R. W. Stewart and R. W. Burling (1970): Spectra and cospectra of turbulence over water. Quart. J. R. Met. Soc. Vol. 96, pp. 138-143.

Mori, Y., (1980): Spectrum of long period fluctuations of surface wind at Marcus Island, Mon. Wea. Rev., Vol. 108 (Sept.), pp. 1456-1461.

Neumann, G. and W. J. Pierson (1966): Principles of Physical Oceanography. Printice Hall Englewood Cliffs, NJ. 545 pp

Pierson, W. J., (1981 a): Recommendations for improved and extended wind measurement capabilities by the National Data Buoy System. The City University of New York, Institute Marine and Atmospheric Sciences. Tech. Report Prepared for Computer Sciences Corporation, NSTL STA., Miss.

Pierson, W. J. (1981 b): The variability of winds over the ocean in Beal, R., P. S. DeLeonibus and I. Katz Eds Spaceborne Synthetic Aperture Radar for Oceanography. Johns Hopkins. University Press The Johns Hopkins Oceanographic Studies, No. 7.

Pierson, W. J., S. Peteherych, and J. C, Wilkerson (1980): The winds of the comparison data set for the Seasat Gulf of Alaska experiment, IEEE Journal of Ocean Engineering Vol. OE5 No. 2 April pp. 169-176.

Pierson, W. J. and R. E. Salfi (1982): Monte Carlo studies of ocean wind vector measurements by SCATT: Objective criteria and maximum likelihood estimates for removal of aliases, and effects of cell size on accuracy of vector winds. The City University of New York Institute of Marine and Atmospheric Sciences, The City College of the City University of New York. NASA Langley Research Center. NASA Contractor Report 165837-1.

Pond, S., G. T. Phelps, J. E. Paquin, G. McBean and R. W. Stewart (1971): Measurements of the turbulent fluxes of momentum moisture and sensible heat over the ocean. J. Atmos. Sci. Vol. 28, No. 6 pp. 901-917.

Reynolds, O. (1894): On the dynamical theory of incompressible viscous fluids and the determination of the criteria. Phil. Trans. Roy. Soc. A Vol. 186 p. 123 (London).

Robinson, G. D. (1978a): Weather and climate forecasting as problems in hydrodymanics. Month. Weather Rev. Vol. 106 pp. 448-457.

Robinson, G. D. (1978b): Reply to Laurmann, Month. Weather Rev. Vol. 106 pp. 448-457.

Schroeder, L. C., D. H. Boggs, G. Dome, I. M. Halberstam, W. L. Jones, W. J. Pierson and F. J. Wentz (1982): The relationship between wind vector and normalized radar cross section used to derive SEASAT-A satellite scatterometer winds. J. Geophys. Res. 87, C5, pp. 3318-3336.

Smith, S. D. (1980): Wind stress and heat flux over the ocean for gale force winds. J. Phys. Ocean. Vol. 10, No. 5 (May) pp. 709-736.

Soulsby, R. L. and K. R. Dyer (1981): The form of the near-bed velocity profile in a tidally accelerating flow. J. Geophys. Res. Vol. 86, No. C9 pp. 8067-8074.

Thompson, P. D. (1973): The equilibrium energy spectrum of randomly forced two-dimensional turbulence. J. Atmos. Sci., Vol. 30, No. 8 Nov. pp. 1593-1598.

Van Der Hoven, I. (1957): Power spectrum of horizontal wind speed in the frequency range from 0.007 to 900 cycles per hour. J. Meteorol. 14 pp. 160-164.

1 Report No	2 Government Accession No	3. Recipient's Catalog No
NASA CR-166041		

4 Title and Subtitle	5 Report Date
The Measurement of the Synoptic Scale Wind Over the Ocean	December 1982
	6 Performing Organization Code

7 Author(s)	8 Performing Organization Report No
Willard J. Pierson	
	10 Work Unit No

9 Performing Organization Name and Address	11 Contract or Grant No
CUNY Institute of Marine and Atmospheric Science at the City College Convent Avenue at 138th Street, New York, NY 10031	NAS1-15669 and NAGW-266

12 Sponsoring Agency Name and Address	13 Type of Report and Period Covered
National Aeronautics and Space Administration Washington, DC 20546	Contractor Report 1981-1982
	14 Sponsoring Agency Code

15 Supplementary Notes

Langley technical monitor: Lyle C. Schroeder
Topical Report

16 Abstract

Mesocale and microscale features of the turbulent winds over the ocean are related to the synoptic scale winds in terms of published spectral forms for the microscale, a mesoscale valley and published values of U_*, VAR u', VAR v' and z/L, as defined in the text and as obtained for moderate to gale force winds. The frequencies involved correspond to periods longer than 1 hour and extend to the microscale, which starts at a period near 2 minutes, or so, and continues to the Kolmogorov inertial range.

Non dimensional spectra that span both the mesoscale and the microscale are derived as a function of u_*, $f(= n\ z/\bar{u})$ and z/L, where z is 10 meters, L is the Monin Obukov stability length and $\bar{u}$ is evaluated at 10 meters. For the same $\bar{u}$, different values of z/L produce a range of values of u_* which in turn result in variations of the eddy structure of the mesoscale and microscale spectra.

Both conventional anemometer averages and remotely sensed winds contain a random component of the mesoscale wind in their values. These components are differences and not "errors" when winds are compared, and quantitative values for these differences are given. Ways to improve the measurement of the synoptic scale wind by transient ships, data buoys and scatterometers on future spacecraft are described. These ways are longer averaging times for ships and data buoys, depending on the synoptic conditions, and pooling spacecraft data to form super observations. Design considerations for future remote sensing systems are given.

17 Key Words (Suggested by Author(s))	18 Distribution Statement
Synoptic Scale Winds Mesoscale Variability Microscale Variability Conventional Anemometer Remotely Sensed Winds Future Remote Sensors	Unclassified - Unlimited Star Category 48

19 Security Classif (of this report)	20 Security Classif (of this page)	21 No of Pages	22 Price
UNCLASSIFIED	UNCLASSIFIED	80	A05

For sale by the National Technical Information Service, Springfield, Virginia 22161

End of Document